AN INVESTIGATION OF THE DISTRIBUTION OF RADIATION SCATTERED BY OPTICAL SURFACES

Roland V. Shack, et al

Arizona University

Prepared for:

Space and Missile Systems Organization

August 1975

AN INVESTIGATION OF THE DISTRIBUTION OF RADIATION SCATTERED BY OPTICAL SURFACES

Roland V. Shack
James E. Harvey

Optical Sciences Center
The University of Arizona
Tucson, Arizona 85721

August 1975

Final Report for Period October 1973 to December 1974

Approved for public release; distribution unlimited.

Prepared for the
Space and Missile Systems Organization
Air Force Systems Command
Los Angeles, California 90009

This report has been reviewed by the Information Office (OI) and is releasable to the National Technical Information Service (NTIS). At NTIS, it will be available to the General public, including foreign nations.

This technical report has been reviewed and is approved for publication.

EDWARD R. DIETZ, Capt, USAF
Program Manager
Survivability Directorate

FOR THE COMMANDER

JOHN A. NORBY, LtCol, USAF
Director, Survivability Directorate

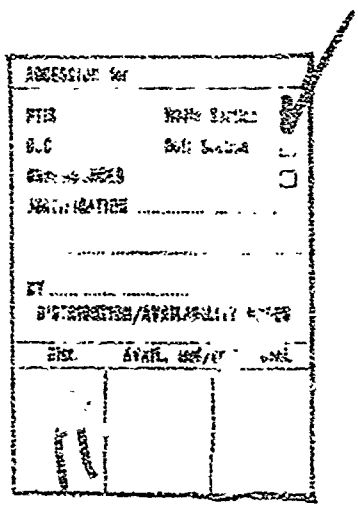

UNCLASSIFIED

SECURITY CLASSIFICATION OF THIS PAGE (When Data Entered)

REPORT DOCUMENTATION PAGE		READ INSTRUCTIONS BEFORE COMPLETING FORM
1. REPORT NUMBER TR #75-236	2. GOVT ACCESSION NO.	3. RECIPIENT'S CATALOG NUMBER
4. TITLE (and Subtitle) AN INVESTIGATION OF THE DISTRIBUTION OF RADIATION SCATTERED BY OPTICAL SURFACES		5. TYPE OF REPORT & PERIOD COVERED Final Report for Period October 1973 to Dec. 1974 6. PERFORMING ORG. REPORT NUMBER
7. AUTHOR(s) Roland V. Shack James E. Harvey		8. CONTRACT OR GRANT NUMBER(s) F04701-74-C-0083
9. PERFORMING ORGANIZATION NAME AND ADDRESS Optical Sciences Center University of Arizona Tucson, Arizona 85721		10. PROGRAM ELEMENT, PROJECT, TASK AREA & WORK UNIT NUMBERS
11. CONTROLLING OFFICE NAME AND ADDRESS Space and Missile Systems Organization Air Force Systems Command Los Angeles, California 90009		12. REPORT DATE August 1975 13. NUMBER OF PAGES 120
14. MONITORING AGENCY NAME & ADDRESS(if different from Controlling Office)		15. SECURITY CLASS. (of this report) Unclassified 15a. DECLASSIFICATION/DOWNGRADING SCHEDULE

16. DISTRIBUTION STATEMENT (of this Report)

Approved for public release; distribution unlimited.

17. DISTRIBUTION STATEMENT (of the abstract entered in Block 20, if different from Report)

18. SUPPLEMENTARY NOTES

19. KEY WORDS (Continue on reverse side if necessary and identify by block number)

Surface Scatter
Diffuse Reflectance
Surface Properties
Optical Surfaces
Diffraction Theory

20. ABSTRACT (Continue on reverse side if necessary and identify by block number)

The direct application of Fourier transform theory to the problem of surface scatter allows the well-known techniques of linear systems theory to be applied to the scattering process. For surfaces with well-behaved statistics, this approach results in a linear, shift-invariant scattering function that does not change shape with variations in the angle of incidence. The apparatus and technique used for measuring the scattered light distribution from a variety of optical surfaces as a function of angle of incidence is discussed,

(Cont'd)

DD FORM 1 JAN 73 1473 EDITION OF 1 NOV 65 IS OBSOLETE
S/N 0102-014-6601

UNCLASSIFIED

SECURITY CLASSIFICATION OF THIS PAGE (When Data Entered)

20. Continued.

and the results of experimental measurements are presented and compared with theoretical predictions.

FOREWORD

This is the final report for the investigation of radiation scattered by optical surfaces by the Optical Sciences Center, University of Arizona, Tucson, Arizona. The work was performed under Air Force Contract FC4701-74-C-0083. The program was carried out under the auspices of the Space and Missile Systems Organization, Air Force Systems Command, Los Angeles, California.

The principal investigator for the Optical Sciences Center was Roland V. Shack. The project engineer and co-investigator was James E. Harvey.

TABLE OF CONTENTS

		Page
I.	INTRODUCTION	1
	Previous Studies of Surface Scattering Phenomena	1
II.	GENERALIZED SCALAR DIFFRACTION THEORY	6
	The Diffracted Wave Field as a Superposition of Plane Waves	7
	Initial Conditions	7
	The Direct Application of Fourier Transform Theory	9
	The Transfer Function of Free Space	10
	The Diffracted Wave Field as a Superposition of Spherical Waves	14
	The Point Spread Function	14
	Huygens' Principle	15
	General Rayleigh-Sommerfeld Diffraction Formula	16
	Geometrical Configurations of the Observation Space	17
	The Diffracted Wave Field on a Plane	17
	The Diffracted Wave Field on a Hemisphere	19
	Aberrations of Diffracting Systems	22
	Shift Invariance of the Diffracted Wave Field	28
	Summary	32
III.	SURFACE SCATTER THEORY	35
	Surface Scatter Phenomena as a Diffraction Process	35
	Effect of the Scattering Surface upon the System Pupil Function	36
	Scattered Wave Field on a Hemisphere	38
	The Effective Spread Function of a Scattering System	39
	Scattering from Optical Surfaces	39
	Assumptions Concerning the Statistical Properties of an Optical Surface	41
	The Effective Transfer Function of a Scattering Surface	42
	The Effective Spread Function of a Scattering Surface	45

TABLE OF CONTENTS--*Continued*

Page

Relationship between the Spread Function and the BRDF 47
Shift Invariance in Direction Cosine Space 48

IV. SURFACE SCATTER MEASUREMENTS 51

Apparatus 51
The Light Source 51
The Detector Unit 54
The Scanning Mechanism 60
The Incident Beam 60
Experimental Procedures 60
Sample Preparation 64
System Alignment 66
Measurement Technique 68
Data and Results 71

V. SURFACE STRUCTURE MEASUREMENTS 78

Electron Microscopy 78
FECO Interferometry 82

VI. SUMMARY 83

APPENDIX A. FRESNEL AND FRAUNHOFER DIFFRACTION 86

APPENDIX B. CALCULATION OF ABERRATION COEFFICIENTS FOR DIFFRACTED WAVE FIELDS 89

APPENDIX C. BIDIRECTIONAL REFLECTANCE DISTRIBUTION FUNCTION . . . 94

APPENDIX D. LITERATURE REVIEW 97

LIST OF ILLUSTRATIONS

Figure		Page
1.	Schematic Representation of Scattering from a Rough Surface	2
2.	Geometry of Planes P_O and P	8
3.	Unit Circle in Direction Cosine Space	12
4.	(a) Original Disturbance Separated into its Propagating and Evanescent Parts. (b) Direction Cosine Spectrum Separated into its Propagating and Evanescent Parts	13
5.	Geometrical Relationship between Incident Beam, Diffracting Aperture, and Observation Hemisphere	20
6.	Diffraction Pattern of a 10-Line per mm Ronchi Ruling Placed in an f/6 Cone of Light with a 40-mm Diameter	27
7.	Diffraction Pattern of a 10-Line per mm Ronchi Ruling Placed in an f/20 cone of Light with a 12-mm Diameter	29
8.	Geometrical Configuration when the Incident Beam Strikes the Diffraction Aperture at an Arbitrary Angle	31
9.	Illustration of the Position of the Diffracted Orders in Real Space and Direction Cosine Space	33
10.	Graphical Illustration of Surface Height Variations and Associated Statistical Parameters	37
11.	An Ensemble of Two-Dimensional Sample Functions $\hat{W}_i(\hat{x},\hat{y})$ Representing Surface Height Variations Constitutes a Random Process $\hat{W}(\hat{x},\hat{y})$	40
12.	(a) Effective Transfer Function of a Scattering Surface. (b) Spread Function Associated with a Scattering Surface	46

LIST OF ILLUSTRATIONS--*Continued*

Figure		Page
13.	Geometrical Relationship between Incident Beam, Scattering Surface, the Measured Scattered Light Distribution, and the Resulting Spread Function	49
14.	Schematic Diagram of Scatter Measurement Apparatus	52
15.	Apparatus for Measuring Scattered Light Distribution from Optical Surfaces	53
16.	(a) Previous Configuration of Detector Probe Unit. (b) New Configuration of Detector Probe Unit	55
17.	Detailed Illustration of New Fiber-Optic Probe	57
18.	Detector Response as a Function of Field Angle for Detector Configurations Shown in Fig. 16	58
19.	Photomultiplier Tube Linearity Curve	59
20.	Detailed Illustration of Movable Arm Supporting the Optical System Forming Incident Beam	61
21.	Geometrical Configuration of Two Principal Planes in which the Scattered Light Field will be Sampled	63
22.	(a) Spread Function of Incident Beam. (b) Spread Function of Scattering Surface. (c) Spread Function of Scattering System	70
23.	Comparison of Scatter Profiles for Different Incident Angles	72
24.	Comparison of Scatter Profiles Taken in Different Directions for an Incident Beam at 45 Degrees	74
25.	Comparison of Scatter Profiles for Samples with a Wide Range of Surface Roughnesses for a Normally Incident Beam	76
26.	Comparison of Scatter Profiles from Special Materials and Unusual Fabrication Techniques with Those of Conventional Optical Surfaces	77

LIST OF ILLUSTRATIONS--*Continued*

Figure		Page
27.	(a) Typical Electron-Micrograph Stereo Pair of a Ground Glass Surface. (b) Surface Profile of Ground Glass Sample as Determined by Stereo-Photogrammetric Techniques	79
28.	Surface Profile of Ground Glass Sample and its Associated Surface Height Distribution and Autocorrelation Function	81
29.	Geometry of Incident and Reflected Elementary Beams used to Define the Bidirectional Reflectance Distribution Function	95

LIST OF TABLES

Table Page

1. Tabulation of Expressions for the Aberration Coefficients for Several Different Geometrical Configurations of (a) Incident Wavefront, and (b) Observation Space 24

2. Surface Preparation Techniques 65

CHAPTER I

INTRODUCTION

With the recent refinement of optical devices and systems there has evolved a need to examine in closer detail the mechanism and properties of optical scattering. The relationship between surface microroughness and radiant energy scattering has an important bearing on the cost and performance of optical systems. The surface roughness and resulting light scattering properties are therefore important characteristics of any material considered for use as an optical element. Moreover, if the scattering mechanism were completely understood, surface preparation techniques could possibly be changed to save both time and expense.

Previous Studies of Surface Scattering Phenomena

If a propagating wave is incident upon a plane surface, the reflected wave is concentrated in the specular direction as determined by the well-known laws of reflection [Born and Wolf (1959)]. Another idealized surface is the perfectly diffuse reflector which scatters light according to Lambert's cosine law [Hudson (1969)]. A more physically realistic situation is shown in Fig. 1, which illustrates the optical scattering that occurs when light is reflected from a rough surface. If the surface is not too rough the reflected light is seen to

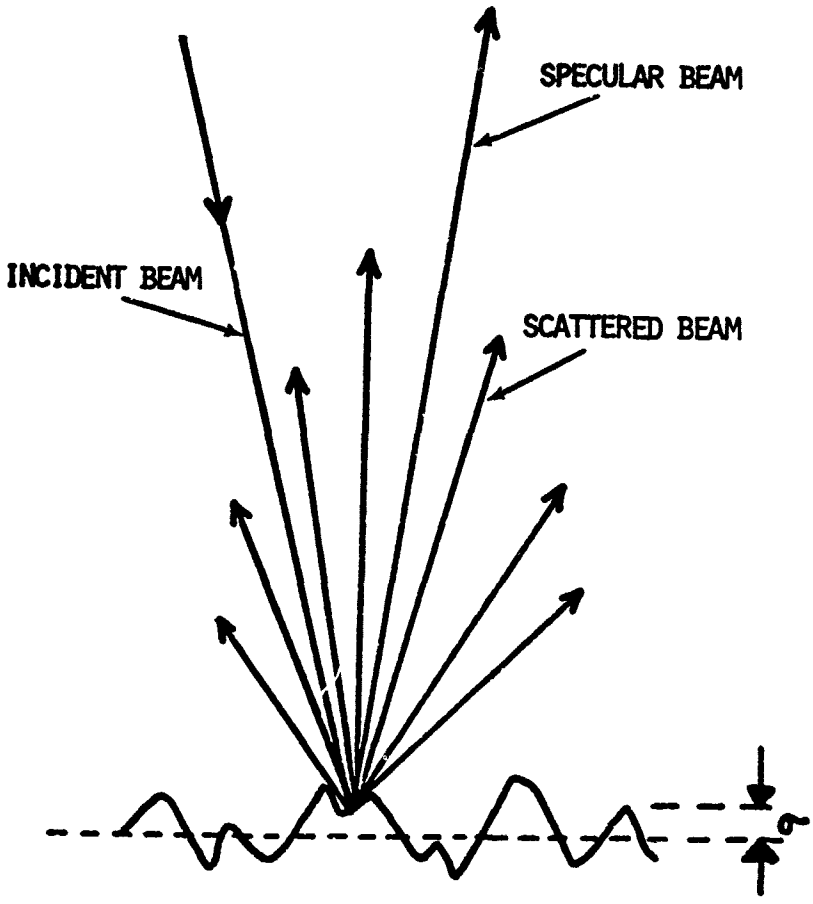

Fig. 1. Schematic Representation of Reflectance from a Rough Surface.

consist of a specular component and a diffuse component which is scattered over a wide range of angles centered upon the specular beam.

One of the earliest investigators of scattering from a rough surface was Lord Rayleigh. In 1896 [Rayleigh (1945)] he was investigating the reflection of acoustic waves, and later [Rayleigh (1901)] he noted the effects of poorly polished surfaces on optical performance. His work examined the effects of surface roughness, wavelength, and angle of incidence on the reflected beam. Chenmoganadam (1919) derived a theory of scattered light based on the phase shift of the reflected beam due to the rough surface.

However, it was not until the problem of background clutter in radar applications became apparent that a determined effort was made to solve the scattering problem for random surfaces. For example, scattering from the sea motivated the work of Davies (1954) as well as others [Blake (1950), Barrick (1970), Bass (1968), Beard (1961), and Fuks (1966)]. Considerable work has also been done in attempts to explain radar reflection from the moon [Daniels (1961), Evans and Pettengill (1963), Fung (1964, 1967), Hagfors (1964)].

Random rough surfaces can be classified into two main groups. Rough surfaces made up of a random array of objects or shapes with known scattering characteristics were investigated by Ament (1960), Twersky (1957), Spetner (1958), and Peake (1959). The other approach treats the rough surface as a stochastic process. This approach was taken by Isakovich (1952), Ament (1953), Eckart (1953), Feinstein (1954), Davies (1954), and Beckmann (1957).

Since optical surfaces clearly fall into the second classification of random surfaces, Bennett and Porteus (1961) expanded and experimentally investigated the scattering theory of Davies (1954). From this and subsequent work [Bennett (1963) and Porteus (1963)] the reflectance properties of samples with a measured surface roughness were directly compared to theory with good results. Interest in these measurements led to investigations at the Optical Sciences Center by McKenney (1972), Mott (1971), Orme (1972) and DeBell (1974).

In the above studies, satisfactory theories have been developed only for the two limiting cases of very rough surfaces ($\sigma/\lambda >> 1$) and very smooth surfaces ($\sigma/\lambda << 1$). Until recently most of the efforts have been confined to very smooth optical surfaces which satisfy the second condition. However, recent applications require a more general theoretical treatment.

In this study surface scatter phenomena is treated as a diffraction process where the scattering surface introduces an isotropic random wavefront disturbance. The Fourier techniques of linear systems theory, which have been applied to the problem of image formation through a turbulent atmosphere by Shack (1967), are then utilized to develop a surface scattering theory. Experimental measurements are also made in an attempt to verify this theory.

Early work in the development of the above theory was carried out under Contract F04701-72-C-0181 and is documented along with

experimental results in "Surface Scatter Study," Technical Report SAMSO TR 74-8[illegible], dated February 1974. An update of the literature review accomplished under that contract is included in this report.

CHAPTER II

GENERALIZED SCALAR DIFFRACTION THEORY

The phenomenon of diffraction involves a wave field incident upon one or more obstacles or apertures of absorbing or conducting surfaces. The calculation of the wave field emerging from such a diffracting system is the goal of all diffraction theories.

It should be emphasized that both the Kirchhoff and Rayleigh-Sommerfeld theories, as well as the present discussion in this paper, treats light as a scalar phenomenon. (For a detailed treatment of the historical development of diffraction theory, see Goodman (1968), pp. 30-56.) Such an approach entirely neglects the fact that the various components of the electric and magnetic field vectors are coupled through Maxwell's equations and cannot be treated independently.

Microwave experiments have shown that scalar theory yields very accurate results provided that: (i) the diffracting aperture is large compared to a wavelength, and (ii) the diffracted wave field is observed far from the aperture. It is significant that although the present treatment is limited by being a scalar theory, the above approximations need not be imposed during the mathematical formulation as they are in the Kirchhoff theory, or in its subsequent use as they almost always are with the Rayleigh-Sommerfeld theory. The following development

threfore provides much more insight and accuracy than the conventional treatments.

The Diffracted Wave Field as a Superposition of Plane Waves

The fundamental diffraction problem basically consists of two parts: (i) determining the effect of introducing the diffracting screen upon the field immediately behind the diffracting screen, and (ii) how does it affect the field downstream from the diffracting screen (i.e., what is the field immediately behind the diffracting screen and how does it propagate).

Consider first the propagation problem and let the complex amplitude distribution of the optical disturbance in plane P_o be represented by the scalar function $U_o(\hat{x},\hat{y};0)$. This scalar disturbance in P_o will be considered the only radiation contributing to the field $U(\hat{x},\hat{y};\hat{z})$ in plane P (see Fig. 2). $\hat{z}$ has a parametric relationship since it is a function of the observation plane. Note that a scaled coordinate system is utilized in which $\hat{x} = x/\lambda$, $\hat{y} = y/\lambda$, $\hat{z} = z/\lambda$.

Initial Conditions

It will be assumed that the complex amplitude of any monochromatic optical disturbance propagating through free space must obey the time-independent wave equation (Helmholtz equation). We will also assume that the Fourier transform of the scalar field $U_o(\hat{x},\hat{y};0)$ exists. This is not a severe restriction, however, as Bracewell (1965) points

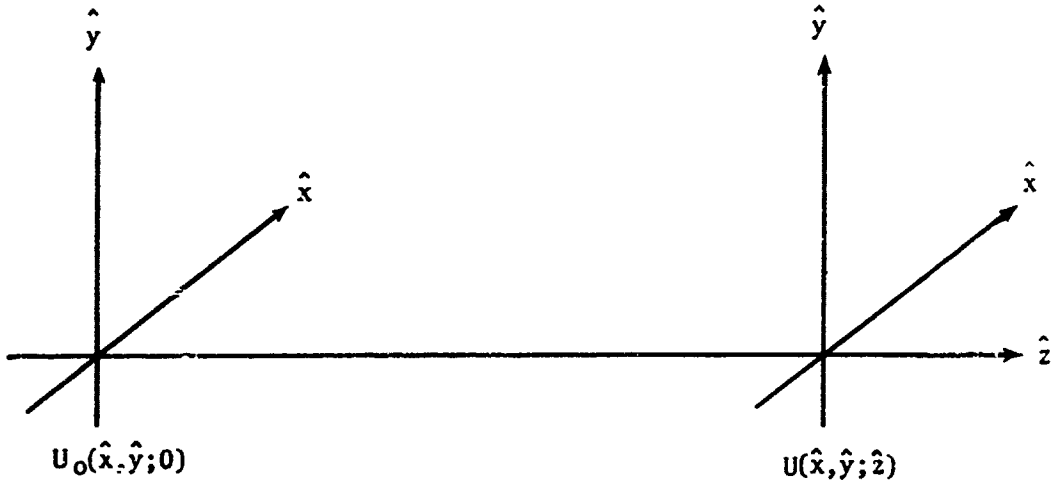

Fig. 2. Geometry of Planes P_0 and P.

out that physical possibility is a valid sufficient condition for the existence of a Fourier transform.

The Direct Application of Fourier Transform Theory

We can thus define the following Fourier transform relationships that exist for planes P_o and P.

$$A_o(\alpha,\beta;0) = \iint_{-\infty}^{\infty} U_o(\hat{x},\hat{y};0)e^{-i2\pi(\alpha\hat{x}+\beta\hat{y})}d\hat{x}d\hat{y} \tag{1}$$

$$U_o(\hat{x},\hat{y};0) = \iint_{-\infty}^{\infty} A_o(\alpha,\beta;0)e^{i2\pi(\alpha\hat{x}+\beta\hat{y})}d\alpha d\beta \tag{2}$$

$$A(\alpha,\beta;\hat{z}) = \iint_{-\infty}^{\infty} U(\hat{x},\hat{y};z)e^{-i2\pi(\alpha\hat{x}+\beta\hat{y})}d\hat{x}d\hat{y} \tag{3}$$

$$U(\hat{x},\hat{y};\hat{z}) = \iint_{-\infty}^{\infty} A(\alpha,\beta;\hat{z})e^{i2\pi(\alpha\hat{x}+\beta\hat{y})}d\alpha d\beta. \tag{4}$$

Equations (2) and (4) indicate that the monochromatic scalar wave field in planes P_o and P can be decomposed into plane wave components whose amplitudes are a function of the direction cosines of the propagation vector. The functions $A_o(\alpha,\beta;0)$ and $A(\alpha,\beta;\hat{z})$ will be referred to as the direction cosine spectrum of plane waves contributing to the disturbance $U_o(\hat{x},\hat{y};0)$ and $U(\hat{x},\hat{y};\hat{z})$ respectively. The direction cosine

spectrum of plane waves is used here in lieu of the angular spectrum of plane waves discussed by Ratcliff (1956) and others. This is consistent with a more general treatment which is not restricted to small angles.

In the scaled coordinate system $\hat{\nabla}^2 = \lambda^2\nabla^2$, and $\hat{k}^2 = \lambda^2 k^2 = (2\pi)^2$. Hence the Helmholtz equation becomes

$$[\hat{\nabla}^2 + (2\pi)^2]U(\hat{x},\hat{y};\hat{z}) = 0. \tag{5}$$

Now applying Eq. (4) and requiring the individual plane wave components to satisfy the Helmholtz equation, we find

$$A(\alpha,\beta;\hat{z}) = A_O(\alpha,\beta;0)e^{i2\pi\gamma\hat{z}} \tag{6}$$

where

$$\gamma = \sqrt{1 - \alpha^2 - \beta^2}.$$

The Transfer Function of Free Space

Since Eq. (6) relates the Fourier transforms of the scalar fields in planes P_O and P it can be rewritten in terms of a transfer function for free space, $H(\alpha,\beta;\hat{z})$

$$H(\alpha,\beta;\hat{z}) \equiv \frac{A(\alpha,\beta;\hat{z})}{A_O(\alpha,\beta;0)} = e^{i2\pi\gamma\hat{z}}. \tag{7}$$

We have thus far applied no restrictions on γ and two regions of interest are apparent: that for real values of γ and that for imaginary values.

$$\gamma = \sqrt{1 - (\alpha^2+\beta^2)} \begin{cases} \text{for } (\alpha^2 + \beta^2) \leq 1 & \gamma \text{ is } \underline{\text{real}} \\ \text{for } (\alpha^2 + \beta^2) > 1 & \gamma \text{ is } \underline{\text{imaginary}}. \end{cases} \tag{8}$$

Consider now a unit circle in the α-β plane of direction cosine space as shown in Fig. 3. Inside this unit circle γ is real and the corresponding part of the disturbance will propagate and contribute to the wave field in plane *P*. However, those components of the direction cosine spectrum which lie outside the unit circle have imaginary values of γ and represent that part of the disturbance which experiences a rapid exponential decay. This is the part of the disturbance which is commonly referred to as the <u>evanescent wave</u> [Goodman (1968)].

Let $U_O(\hat{x},\hat{y};0)$ be the product of the complex amplitude transmittance of a diffracting screen and the complex amplitude distribution incident upon it. Figure 4a illustrates this quantity broken down into the part which propagates and the part which makes up the evanescent wave for the case of a unit amplitude plane wave normally incident upon a circular aperture. The direction cosine spectrum of plane waves associated with these respective optical disturbances are shown in Fig. 4b.

Note that the sharp corners on the original disturbance in Fig. 4a correspond to Kirchhoff's unwarranted boundary conditions. It is the propagating part <u>only</u> that accurately represents the disturbance

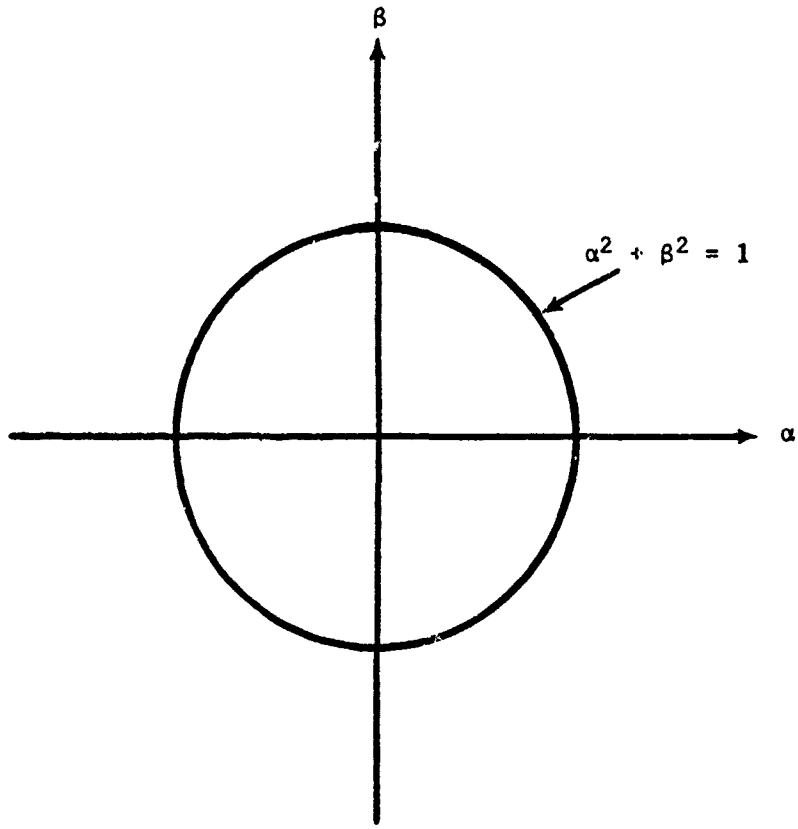

Fig 3. Unit Circle in Direction Cosine Space.

The plane wave components inside this circle will propagate, and the plane wave components outside this circle contribute to the evanescent wave.

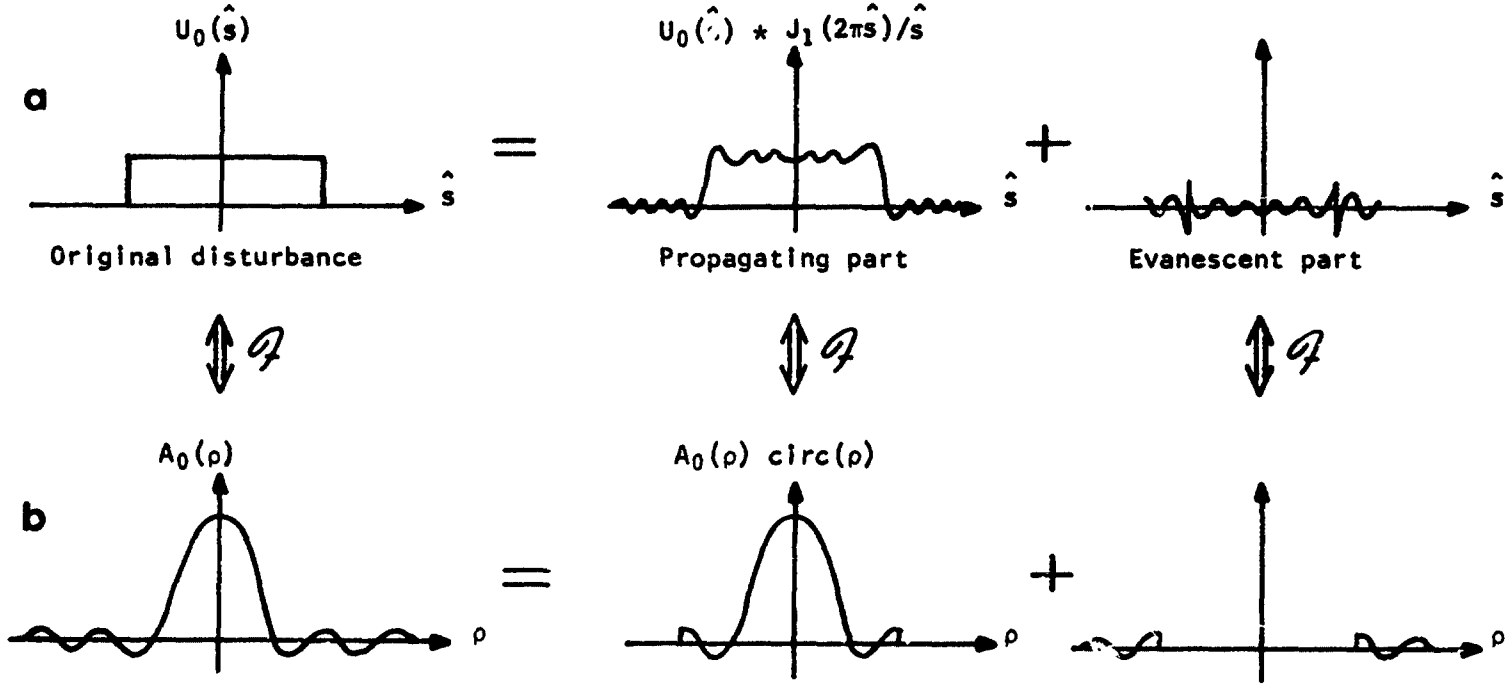

Fig. 4. (a) Original Disturbance Separated into Its Propagating and Evanescent Parts. (b) Direction Cosine Spectrum Separated into Its Propagating and Evanescent Parts.

immediately behind the diffracting aperture which will contribute to the disturbance downstream.

It is now clear that the complex amplitude distribution in plane P can be determined by Fourier transforming the original disturbance $U_O(\hat{x},\hat{y};0)$, then multiplying the resulting direction cosine spectrum of plane waves $A_O(\alpha,\beta;0)$ by the transfer function of free space given in Eq. (7), and finally by applying the inverse Fourier transform integral of Eq. (4). However, the limits of integration on Eq. (4) must be changed such that the integration is performed only over the unit circle instead of over the entire α-β plane.

The above analysis, in which an optical disturbance is represented as a superposition of plane waves, corresponds to the transfer function approach in image formation and yields considerable insight into the behavior of these plane wave components during the phenomenon of diffraction.

The Diffracted Wave Field as a Superposition of Spherical Waves

The convolution theorem [Bracewell (1965)] of Fourier transform theory requires that a convolution operation exists in the domain of real space that is equivalent to Eq. (6).

The Point Spread Function

We thus have the alternative method of expressing the complex amplitude distribution in the observation plane by the convolution of

the original disturbance with a point spread function. The point spread function is obtained by taking the inverse Fourier transform of the transfer function found in Eq. (7).

Starting with the well-known Weyl expansion formula [Weyl (1919)], Lalor (1968) obtained a result which, with straightforward modification, yields

$$\frac{\partial}{\partial \hat{z}}\left[\frac{e^{i2\pi\hat{r}}}{\hat{r}}\right] = -2\pi \iint_{-\infty}^{\infty} e^{i2\pi\gamma\hat{z}}\, e^{i2\pi(\alpha\hat{x}+\beta\hat{y})}\, d\alpha d\beta, \tag{9}$$

where

$$\hat{r}^2 = \hat{x}^2 + \hat{y}^2 + \hat{z}^2.$$

Hence the appropriate point spread function is given by

$$h(\hat{x},\hat{y};\hat{z}) = \mathcal{F}^{-1}\left\{e^{i2\pi\gamma\hat{z}}\right\} = \left(\frac{1}{2\pi\hat{r}} - i\right)\frac{\hat{z}}{\hat{r}}\,\frac{e^{i2\pi\hat{r}}}{\hat{r}}\,. \tag{10}$$

Huygens' Principle

Recall now the assertion by Christiaan Huygens [Thompson (1912)] in 1678 that each element of a wavefront may be regarded as the center of a secondary disturbance which gives rise to spherical wavelets; and moreover that the position of the wavefront at any later time is the envelope of all such wavelets. These intuitive convictions, sometimes called Huygens' wavefront construction, are an excellent description of

a convolution operation in which the initial disturbance is convolved with a Huygens' wavelet. It is therefore quite appropriate to think of the point spread function of a diffraction system as the intersection of a Huygens' wavelet with the observation plane.

Equation (10) is therefore an exact mathematical expression for a Huygens' wavelet which is valid right down to the initial disturbance itself. However, for $\hat{r} \gg 1$,

$$h(\hat{x},\hat{y};\hat{z}) = -i(\hat{z}/\hat{r})\,\frac{e^{i2\pi\hat{r}}}{\hat{r}} = (\hat{z}/\hat{r})\,\frac{e^{i2\pi(\hat{r}\,-\,1/4)}}{r}, \qquad (11)$$

it reduces to the familiar expression for a spherical wave with cosine obliquity factor and a $\pi/2$ phase delay.

General Rayleigh-Sommerfeld Diffraction Formula

If we write down the convolution integral for the disturbance in the observation plane, using the expression in Eq. (10) for $h(\hat{x},\hat{y};\hat{z})$, we obtain the general Rayleigh-Sommerfeld diffraction formula

$$U(\hat{x},\hat{y};\hat{z}) = \iint_{-\infty}^{\infty} U_o(\hat{x}',\hat{y}';0)\left(\frac{1}{2\pi\hat{\ell}} - i\right)\hat{z}/\hat{\ell}\,\frac{e^{i2\pi\hat{\ell}}}{\hat{\ell}}\,d\hat{x}'d\hat{y}' \qquad (12)$$

where

$$\hat{\ell}^2 = (\hat{x}-\hat{x}')^2 + (\hat{y}-\hat{y}')^2 + \hat{z}^2. \qquad (13)$$

This is an exact expression for the diffracted wave field which is valid throughout the entire space in which the diffraction occurs--right down

to the aperture. No approximations have been made. Furthermore, the above equation expresses the disturbance on the observation plane as a superposition of spherical waves which corresponds to the spread function approach in image formation.

Geometrical Configurations of the Observation Space

In order to insure a space invariant point spread function our equations have been restricted to mapping an optical disturbance from an input plane to an output plane, where $\hat{z}$ has a parametric relationship since it is a function of the output plane. However, the summation of these Huygens' wavelets is valid over any surface. The above treatment thus gives us a far more powerful conceptual tool than provided by the equations themselves.

We will therefore investigate the properties of the diffracted wave field on two particular geometrical configurations of the observation surface.

The Diffracted Wave Field on a Plane

Equation (12) reduces to the more familiar but less general form of the Rayleigh-Sommerfeld diffraction formula [Goodman (1968)] when $\hat{z} >> 1$. If we then make the following algebraic substitutions

$$\hat{\ell} = \hat{z}(1 + \delta), \qquad \delta = \frac{\hat{\ell} - \hat{z}}{\hat{z}}, \tag{14}$$

Eq. (12) can be rewritten as

$$U(\hat{x},\hat{y};\hat{z}) = \frac{e^{i2\pi\hat{z}}}{i\hat{z}} \iint_{-\infty}^{\infty} U_o(\hat{x}',\hat{y}';0)\, \frac{1}{(1+\delta)^2}\, e^{i2\pi(\hat{\ell}-\hat{z})}\, d\hat{x}'d\hat{y}'. \tag{15}$$

Note that we have imposed no restriction upon the size of the aperture or the size of the observation space. The only limitation on the above equation is that the observation plane must be many wavelengths from the aperture.

The above diffraction formula is a rather unwieldy integral to solve explicitly for most problems of practical interest. Diffraction pattern calculations are greatly simplified by using the Fresnel or Fraunhofer diffraction formula (see Appendix A); however, severe restrictions are then imposed upon the size of the aperture and the region over which the calculations are valid in the observation plane.

In order that we do <u>not</u> impose these restrictions, let us make a binomial expansion of the quantity $\hat{\ell}$ in the exponent of Eq. (15). We can then rewrite Eq. (15) as the following Fourier transform integral

$$U(\hat{x},\hat{y};\hat{z}) = \frac{e^{i2\pi\hat{z}}}{i\hat{z}} \iint_{-\infty}^{\infty} \mathcal{U}_o(\hat{x}',\hat{y}';\hat{x},\hat{y})\, e^{-\frac{i2\pi}{\hat{z}}(\hat{x}'\hat{x}+\hat{y}'\hat{y})}\, d\hat{x}'d\hat{y}', \tag{16}$$

where the complex quantity

$$\mathcal{U}_o(\hat{x}',\hat{y}';\hat{x},\hat{y}) = T_o(\hat{x}',\hat{y}';0)\, \frac{1}{(1+\delta)^2}\, e^{i2\pi\hat{W}}, \tag{17}$$

can be regarded as a <u>generalized pupil function</u>. All of the terms from the binomial expansion for the quantity $\hat{\ell}$, except for the term which was

extracted for use as the Fourier kernel, are lumped together in the quantity $\hat{W}$ along with any phase variations in the incident wavefront.

Equation (16) clearly reduces to the conventional Fresnel diffraction formula when a plane wave is incident upon the aperture and when $\hat{z}$ is sufficiently large such that $\hat{\ell}$ is adequately approximated by retaining only the first two terms of the binomial expansion.

The Diffracted Wave Field on a Hemisphere

Let us now examine the diffracted wave field on a hemisphere centered upon the diffracting aperture as illustrated in Fig. 5. The position of an arbitrary observation point will be specified by the direction cosines α and β of its position vector, and the radius $\hat{r}$ of the hemisphere upon which it resides. Note that

$$\alpha = \hat{x}/\hat{r}, \quad \beta = \hat{y}/\hat{r}, \quad \text{and} \quad \gamma = \hat{z}/\hat{r}, \tag{18}$$

where

$$\hat{r}^2 = \hat{x}^2 + \hat{y}^2 + \hat{z}^2. \tag{19}$$

With the following algebraic substitutions

$$\hat{\ell} = \hat{r}(1+\varepsilon); \qquad \varepsilon = (\hat{\ell}-\hat{r})/\hat{r}. \tag{20}$$

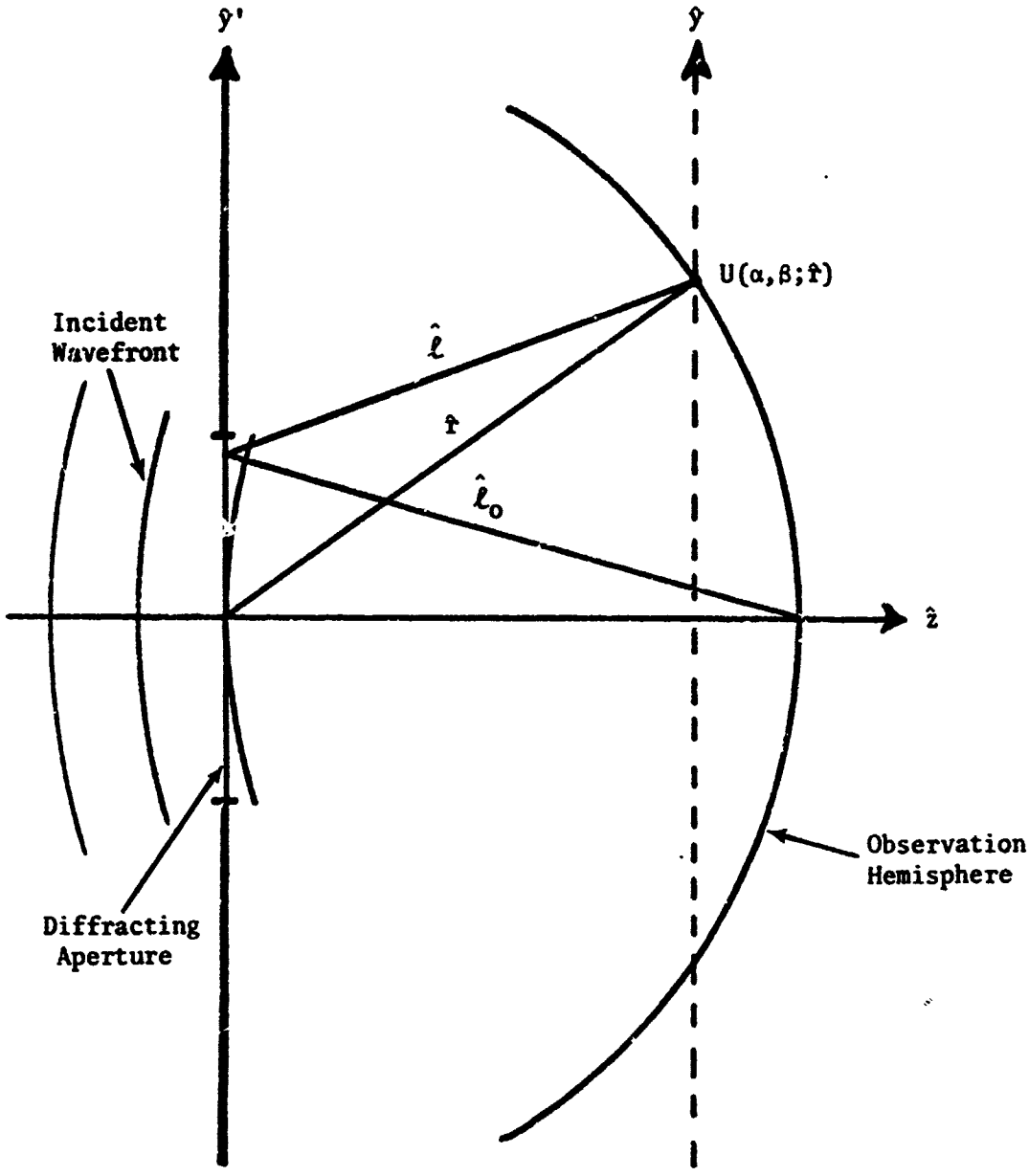

Fig. 5. Geometrical Relationship Between Incident Beam, Diffracting Aperture, and Observation Hemisphere.

Equation (12) can be rewritten as

$$U(\alpha,\beta;\hat{r}) = \gamma \frac{e^{i2\pi\hat{r}}}{\hat{r}} \iint_{-\infty}^{\infty} U_o(\hat{x}',\hat{y}';0) \times \left[\frac{1}{2\pi\hat{r}(1+\epsilon)} - i\right] \frac{1}{(1+\epsilon)^2} e^{i2\pi(\hat{\ell}-\hat{r})} d\hat{x}'d\hat{y}'. \quad (21)$$

We now have an exact expression for the diffracted wave field on an observation hemisphere which is valid throughout the entire half-space behind the plane of the diffracting aperture.

If we now require that $\hat{r} >> 1$ and make the appropriate binomial expansions for the quantity $(\hat{\ell}-\hat{r})$, we again obtain a Fourier transform integral

$$U'(\alpha,\beta;\hat{r}) = \gamma \frac{e^{i2\pi\hat{r}}}{i\hat{r}} \iint_{-\infty}^{\infty} \mathcal{U}_o(\hat{x}',\hat{y}';\alpha,\beta) e^{-i2\pi(\alpha x' + \beta y')} d\hat{x}'d\hat{y}', \quad (22)$$

where the generalized pupil function is given by

$$\mathcal{U}_o(\hat{x}',\hat{y}';\alpha,\beta) = T_o(\hat{x}',\hat{y}';0) \frac{1}{(1+\epsilon)^2} e^{i2\pi\hat{W}}. \quad (23)$$

Once again, all of the terms from the binomial expansion for the quantity $(\hat{\ell}-\hat{r})$, except for the term which was extracted for use as the Fourier kernel, are lumped together in the quantity $\hat{W}$ along with any phase variations in the incident wavefront.

Aberrations of Diffracting Systems

The quantity $\hat{W}$ in Eqs. (17) and (23) represent phase variations in the diffracted wavefront emerging from the aperture. Therefore, $\hat{W}$ can be interpreted as a conventional wavefront aberration function [Hopkins (1950)], which is conveniently expressed as a general power series expansion of the pupil coordinates and the appropriate field parameters.

For the case of a rotationally-symmetric diffracting aperture we can, without loss of generality, choose the observation point to lie on the $\hat{y}$-axis ($\hat{x} = 0$). The wavefront aberration function can then be written as

$$\begin{aligned}\hat{W} = {} & \hat{W}_{200}\rho^2 + \hat{W}_{020}\hat{a}^2 + \hat{W}_{111}\rho\hat{a}\cos\phi \\ & + \hat{W}_{400}\rho^4 + \hat{W}_{040}\hat{a}^4 + \hat{W}_{131}\rho\hat{a}^3\cos\phi + \hat{W}_{222}\rho^2\hat{a}^2\cos^2\phi \\ & + \hat{W}_{220}\rho^2\hat{a}^2 + \hat{W}_{311}\rho^3\hat{a}\cos\phi \\ & + \text{higher-order terms,}\end{aligned} \tag{24}$$

where ρ is a normalized field position of the observation point and $\hat{a}$ is a normalized pupil height.

By equating coefficients of the corresponding terms in the appropriate binomial expansions and the above wavefront aberration function, we obtain expressions for the aberration coefficients in terms of the aperture diameter, the observation distance, and the appropriate field parameter.

The expressions for these aberration coefficients are derived in Appendix B and tabulated in Table 1 to enable easy comparison of several different geometrical configurations of the incident wavefront and the observation space.

Consider first a plane wave illuminating the diffracting aperture and a plane observation space. We see from the first column of Table 1 that all aberrations are present except for lateral magnification error ($\hat{W}_{111}$) which is absent for all geometrical configurations because this term of the binomial expansion for $\hat{\ell}$ is extracted for use as the kernel of the Fourier transform integral. It is clear that very large observation distances are required to reduce defocus ($\hat{W}_{020}$) to a negligible value. Also, distortion ($\hat{W}_{311}$) imposes severe restraints upon the field angle over which the diffracted wave field is accurately described by the Fourier transform of the aperture function. These restrictions are the same as those usually imposed during the development of the Kirchhoff theory and in most applications of the Rayleigh-Sommerfeld diffraction theory.

The effect of illuminating the aperture with a spherical wave converging to the observation plane is to eliminate defocus ($\hat{W}_{020}$) and all orders of spherical aberration ($\hat{W}_{040}$). This removes the requirement for an extremely large observation distance, but the Fourier transform of the aperture function is still valid only over a small region about the optical axis in the observation plane.

Table 1. Tabulation of Expressions for the Aberration Coefficients for Several Different Geometrical Configurations of (a) Incident Wavefront, and (b) Observation Space.

	a. Plane b. Plane	a. Sphere b. Plane	a. Plane b. Hemisphere	a. Sphere b. Hemisphere
Piston Error $\hat{W}_{200}$	$\frac{\hat{s}}{2}\left(\frac{\hat{y}_{max}}{\hat{s}}\right)^2$	$\frac{\hat{s}}{2}\left(\frac{\hat{y}_{max}}{\hat{s}}\right)^2$	0	0
Defocus $\hat{W}_{020}$	$\frac{\hat{s}}{2}\left(\frac{\hat{d}}{2\hat{s}}\right)^2$	0	$\frac{\hat{r}}{2}\left(\frac{\hat{d}}{2\hat{r}}\right)^2$	0
Lateral Magnification Error $\hat{W}_{111}$	0	0	0	0
3rd-Order Piston Error $\hat{W}_{400}$	$-\frac{\hat{s}}{8}\left(\frac{\hat{y}_{max}}{\hat{s}}\right)^4$	$-\frac{\hat{s}}{8}\left(\frac{\hat{y}_{max}}{\hat{s}}\right)^4$	0	0
Spherical Aberration $\hat{W}_{040}$	$-\frac{\hat{s}}{8}\left(\frac{\hat{d}}{2\hat{s}}\right)^4$	0	$-\frac{\hat{r}}{8}\left(\frac{\hat{d}}{2\hat{r}}\right)^4$	0
Coma $\hat{W}_{131}$	$\frac{\hat{s}}{2}\frac{\hat{y}_{max}}{\hat{s}}\left(\frac{\hat{d}}{2\hat{s}}\right)^3$	$\frac{\hat{s}}{2}\frac{\hat{y}_{max}}{\hat{s}}\left(\frac{\hat{d}}{2\hat{s}}\right)^3$	$\frac{\hat{r}}{2}\beta_{max}\left(\frac{\hat{d}}{2\hat{r}}\right)^3$	$\frac{\hat{r}}{2}\beta_{max}\left(\frac{\hat{d}}{2\hat{r}}\right)^3$
Astigmatism $\hat{W}_{222}$	$-\frac{\hat{s}}{2}\left(\frac{\hat{y}_{max}}{\hat{s}}\right)^2\left(\frac{\hat{d}}{2\hat{s}}\right)^2$	$-\frac{\hat{s}}{2}\left(\frac{\hat{y}_{max}}{\hat{s}}\right)^2\left(\frac{\hat{d}}{2\hat{s}}\right)^2$	$-\frac{\hat{r}}{2}\beta_{max}^2\left(\frac{\hat{d}}{2\hat{r}}\right)^2$	$-\frac{\hat{r}}{2}\beta_{max}^2\left(\frac{\hat{d}}{2\hat{r}}\right)^2$
Field Curvature $\hat{W}_{220}$	$-\frac{\hat{s}}{4}\left(\frac{\hat{y}_{max}}{\hat{s}}\right)^2\left(\frac{\hat{d}}{2\hat{s}}\right)^2$	$-\frac{\hat{s}}{4}\left(\frac{\hat{y}_{max}}{\hat{s}}\right)^2\left(\frac{\hat{d}}{2\hat{s}}\right)^2$	0	0
Distortion $\hat{W}_{311}$	$\frac{\hat{s}}{2}\left(\frac{\hat{y}_{max}}{\hat{s}}\right)^3\frac{\hat{d}}{2\hat{s}}$	$\frac{\hat{s}}{2}\left(\frac{\hat{y}_{max}}{\hat{s}}\right)^3\frac{\hat{d}}{2\hat{s}}$	0	0

Choosing the observation space to be a hemisphere centered upon the diffracting aperture eliminates field curvature ($\hat{W}_{220}$), distortion ($\hat{W}_{311}$), and all orders of piston error ($\hat{W}_{200}$ and $\hat{W}_{400}$).

Hence for the case of a spherical incident wave converging to the intersection of the optical axis and an observation hemisphere, only coma ($\hat{W}_{131}$) and astigmatism ($\hat{W}_{222}$) are present. And the values of the aberration coefficients can be calculated from the relationships provided in the last column of Table 1.

Thus, for a system with an aperture diameter of 1 mm and an observation hemisphere with a radius of 1 m, we have for $\lambda = 0.5$ μm and $\beta_{max} = 1$

$$\hat{W}_{131} = 1.25 \times 10^{-4}$$

$$\hat{W}_{222} = -2.50 \times 10^{-1}. \tag{25}$$

Hence there is only $\lambda/4$ of astigmatism at the edge of the field (i.e., 90° field angle).

Similarly for an f/10 system ($\hat{d}/\hat{r} = 0.1$) with an aperture diameter of 5 cm and a maximum field angle of 0.5° ($\beta_{max} = 0.00872$), we have for $\lambda = 0.5$ μm,

$$\hat{W}_{131} = 0.545$$

$$\hat{W}_{222} = -0.095. \tag{26}$$

Hence coma dominates at the edge of the field with a value of approximately $\lambda/2$.

Finally, for an f/10 system with an aperture diameter of 1 cm and a field size equal to the size of the aperture (i.e., a pair of f/10 relay lenses 1 cm in diameter), we have for $\lambda = 0.5$ μm,

$$\hat{W}_{131} = 0.625$$

$$\hat{W}_{222} = -0.625. \tag{27}$$

We find slightly more than $\lambda/2$ of coma and astigmatism at the edge of the field.

It should be pointed out that in each of the above cases the radius of the Airy disc in direction cosine space is approximately equal to $0.001\ \beta_{max}$. Hence the off-axis aberrations are of little more than academic interest unless there is some structure in the aperture with high spatial frequency content which will diffract light at large angles from the direction of the incident beam.

However, the above analysis of the aberrations associated with the diffraction process can be readily applied to holographic systems or systems containing diffraction gratings.

For example, an f/6 system with a 10-line-per-mm Ronchi ruling placed in a 40-mm diameter aperture produces the diffraction pattern shown in Fig. 6. The diffracted order at three different field positions was photographed through a microscope with the following results: at $\beta = 0$ no aberrations were apparent; at $\beta = 0.04$ coma was predominate with a value of approximately 5λ; and at $\beta = 0.10$ coma and astigmatism both have values of approximately 15λ.

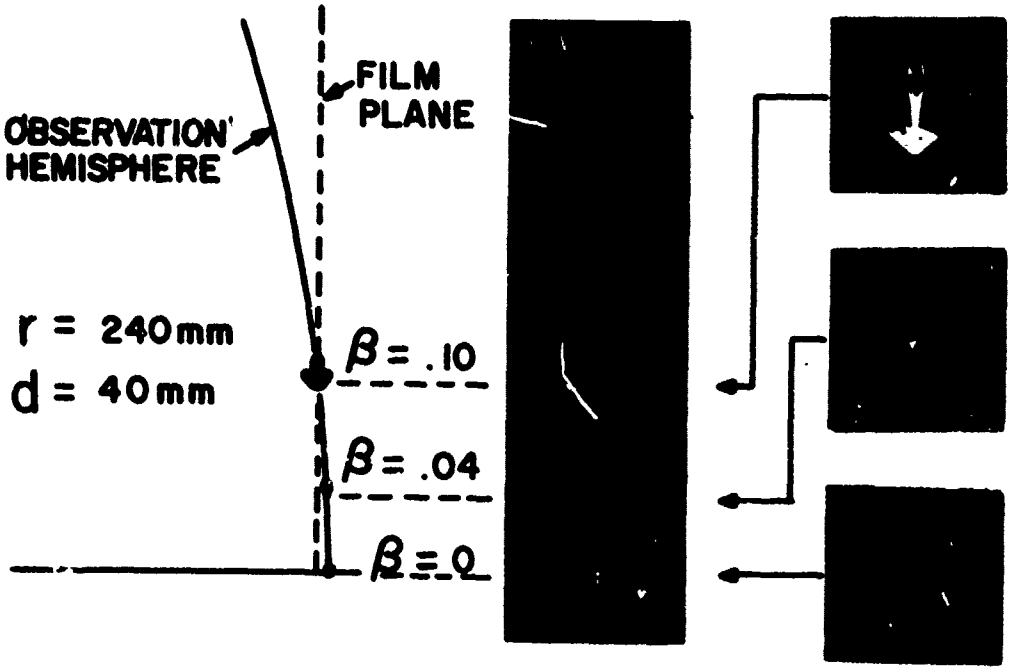

Fig. 6. Diffraction Pattern of a 10-Line per mm Ronchi Ruling Placed in an f/6 Cone of Light with a 40-mm Diameter.

Magnified images of diffracted orders at various field positions indicate that coma is predominant for small field angles with astigmatism also becoming significant at larger field angles.

By stopping the aperture down to a diameter of 12 mm (f/20 system) and observing the diffracted orders at larger field angles, astigmatism becomes the predominate aberration as shown in Fig. 7. The sagittal focus lies on the observation hemisphere of radius r and the medial and tangential surfaces have smaller radii as indicated. The diffracted order at $\beta = .020$ exhibits about 6λ of astigmatism. This order was observed through focus with the microscope and the magnified images are displayed.

In both of the above examples the observed aberrations are in good agreement with those predicted from the coefficients presented in Table 1.

Shift Invariance of the Diffracted Wave Field

We have shown that any departures of the actual diffracted wave field from that predicted by the simple Fourier transform of the aperture function take the form of conventional wavefront aberrations.

If we neglect these aberrations, Eq. (22) reduces to

$$U(\alpha,\beta;\hat{r}) = \gamma \frac{e^{i2\pi\hat{r}}}{i\hat{r}} \iint_{-\infty}^{\infty} T_o(\hat{x}',\hat{y}';0)\ e^{-i2\pi(\alpha\hat{x}'+\beta\hat{y}')}\, d\hat{x}'\, d\hat{y}'. \tag{28}$$

But this is merely the Fourier transform of the aperture function multiplied by a spherical Huygens' wavelet.

$$U(\alpha,\beta;\hat{r}) = \gamma \frac{e^{i2\pi\hat{r}}}{i\hat{r}} \mathcal{F}\{T_o(\hat{x},\hat{y};0)\}. \tag{29}$$

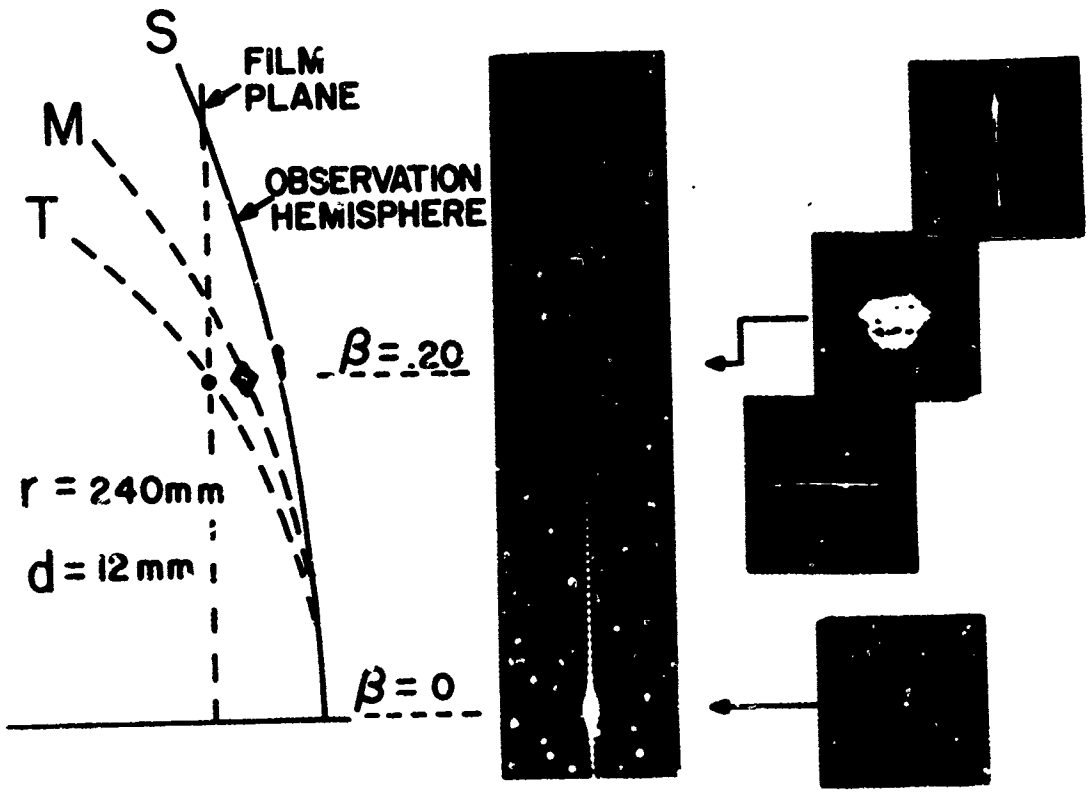

Fig. 7. Diffraction Pattern of a 10-Line per mm Ronchi Ruling Placed in an f/20 Cone of Light with a 12-mm Diameter.

Magnified images of a diffracted order at different focal positions indicate that astigmatism is predominant. The relationship of the sagittal, medial, and tangential surface to the observation hemisphere is also shown.

This relationship is valid provided that the observation space is a hemisphere centered on the diffracting aperture and if the incident radiation is a unit amplitude spherical wave whose center of curvature lies on the intersection of the observation hemisphere with the z-axis. Furthermore, if r is large compared to the size of the diffracting aperture, the Fourier transform relationship is accurate, not merely over a small region about the z-axis, but instead over the entire hemisphere.

Now consider the situation where the incident radiation strikes the diffracting aperture at an angle θ_o as illustrated in Fig. 8. This is equivalent to introducing a linear phase variation across the aperture. By applying the shift theorem [Bracewell (1965)] of Fourier transform theory to Eq. (29) we find that the complex amplitude distribution on the hemisphere is a function of $(\beta - \beta_o)$,

$$U(\alpha,\beta-\beta_o;\hat{r}) = \gamma \frac{e^{i2\pi\hat{r}}}{i\hat{r}} \mathcal{F}\{T(\hat{x},\hat{y};0) \exp[i2\pi\beta_o\hat{y}]\}, \qquad (30)$$

where β is the direction cosine of the position vector of the observation point, and β_o is the direction cosine of the position vector of the undiffracted beam. Note that these direction cosines are obtained by merely projecting the respective points on the hemisphere back on to the plane of the aperture and normalizing to a unit radius. The complex amplitude distribution at an arbitrary point on the hemisphere can now be said to be a function of the distance of the observation point from the undiffracted beam in direction cosine space.

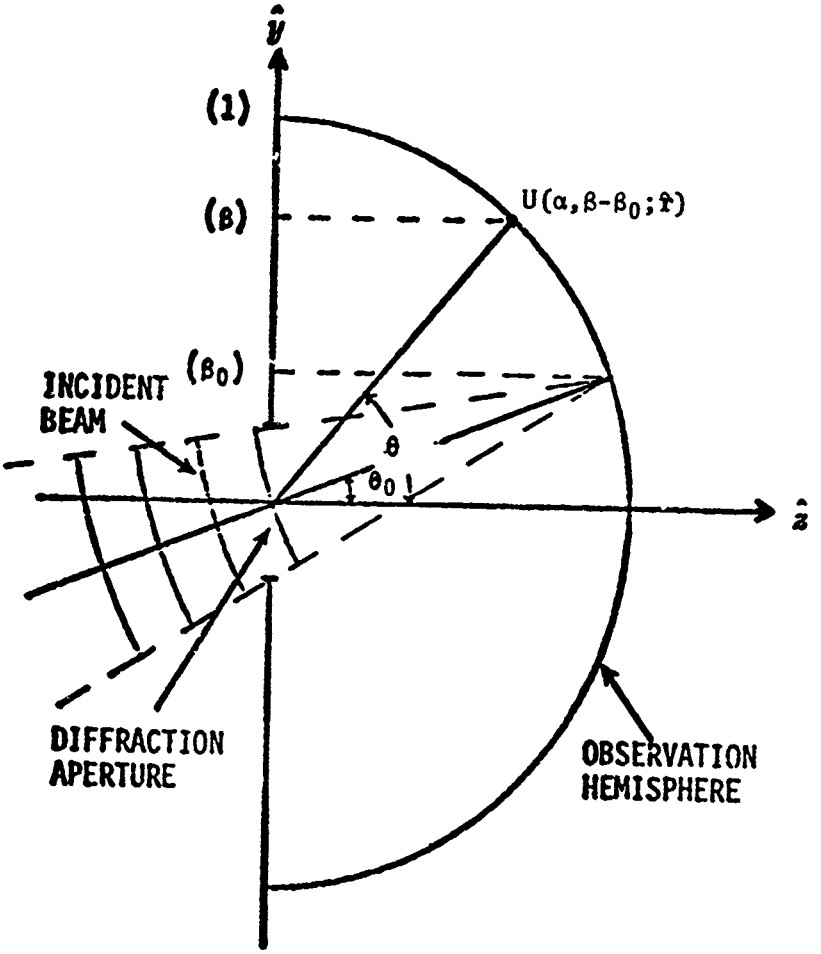

Fig. 8. Geometrical Configuration when the Indicent Beam Strikes the Diffraction Aperture at an Arbitrary Angle.

As a specific example, suppose we have incident light striking a diffraction grating at an angle θ_o. The diffracted orders will strike the observation hemisphere in a cross section which is not a great circle but instead a latitude slice as shown in Fig. 9. Thus for large angles of incidence the various orders appear to lie in a straight line only if they are projected down onto the α-β plane in direction cosine space. It is therefore clear that varying the angle of incidence merely shifts the diffracted wave field in direction cosine space without changing its functional form. This has been verified experimentally by mounting a diffraction grating at the center of a transparent hemisphere, placing graph paper on the plane of the diffraction grating (α-β plane), and scribing appropriate latitude lines on the hemisphere upon which the diffracted orders fall when illuminated with a small laser beam.

Summary

We have developed a very general treatment of scalar diffraction theory that yields more insight and accuracy than the conventional Kirchhoff and Rayleigh-Sommerfeld theories.

By describing the diffraction process in terms of the direction cosines of the propagating light we have obtained the extremely powerful result that the diffracted wave field on an observation hemisphere is given directly by the Fourier transform of the aperture function. This allows us to apply the well-known techniques of linear systems theory that have proven so useful in the area of image formation.

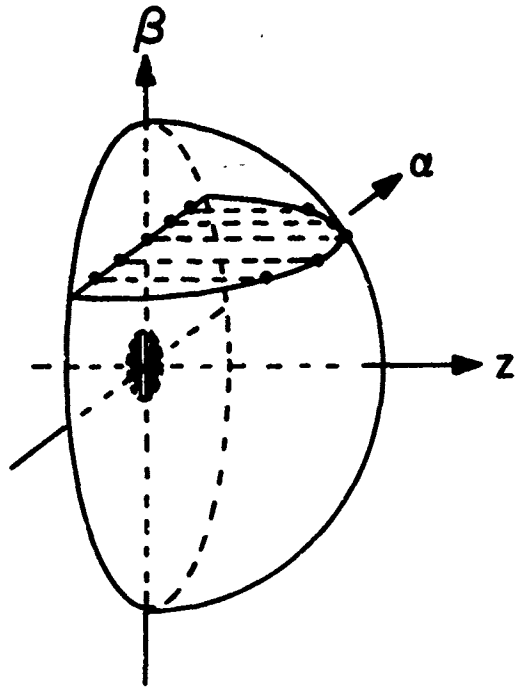

Fig. 9. Illustration of the Position of the Diffracted Orders in Real Space and Direction Cosine Space.

Furthermore, we have shown that any departures of the actual diffracted wave field from that predicted by tne Fourier transform relationship take the form of conventional aberrations whose behavior is well understood in terms of the dimensions of the diffraction aperture, the radius of the observation hemisphere, and the appropriate field parameters.

CHAPTER III

SURFACE SCATTER THEORY

In the following treatment the scattering of light from optical elements is considered to be solely a surface phenomenon. Although it is recognized that bulk scattering mechanisms, such as photon-phonon interactions [Bloembergen (1965)] and scattering from free electrons [Vachaspati (1964)], can exist if the substrate material is not perfectly conducting. Leader and Dalton (1972) have obtained some measured data on the bulk scattering from dielectrics. The excitation of surface plasmons has also been suggested by several investigators as contributing to short wavelength scattering from polished metal surfaces [Beaglehole (1970), Hunderi and Beaglehole (1970), Crowell and Ritchie (1970), Elson and Ritchie (1971), and Daudé, Savary, and Robin (1972)]. However, the above effects are believed to be small for most visible and infrared radiation scattered from metal surfaces.

Surface Scatter Phenomena as a Diffraction Process

In Chapter II it was shown that the diffracted wave field on a hemisphere is given directly by the Fourier transform of the complex amplitude transmittance of the diffracting aperture. In general, the pupil function in a diffracting aperture will include perturbations that lead to scattered radiation. Surface scatter phenomena can thus be

described as a diffraction process in which the pupil function has random phase variations in addition to any existing amplitude variations. The diffraction theory of the previous chapter can therefore be directly applied to the problem of predicting the complex amplitude distribution on an observation hemisphere of radius r resulting from an incident beam of light being reflected from a rough surface.

Effect of the Scattering Surface upon the System Pupil Function

Figure 10 illustrates the surface height variations ($\hat{W}_R$) as a function of distance along the surface. This surface profile has associated with it an autocovariance function and a surface height distribution function as indicated.

The effect of the rough surface can be considered to be a space-dependent modifier, or random component, of the effective pupil function of the system. The disturbance emerging from the scattering surface is given by

$$U_o(\hat{x}\ \hat{y};0) = a_o p(\hat{x},\hat{y};0) = a_o p_L(\hat{x},\hat{y};0) p_R(\hat{x},\hat{y};0). \tag{31}$$

Here the pupil function of the system producing the incident beam is given by

$$p_L(\hat{x},\hat{y};0) = a_L(\hat{x},\hat{y};0)\ e^{i2\pi\hat{W}_L(\hat{x},\hat{y};0)}, \tag{32}$$

where a_L describes the amplitude variations across the exit pupil of the system, and W_L describes any phase variations or aberrations in the wavefront of the incident beam.

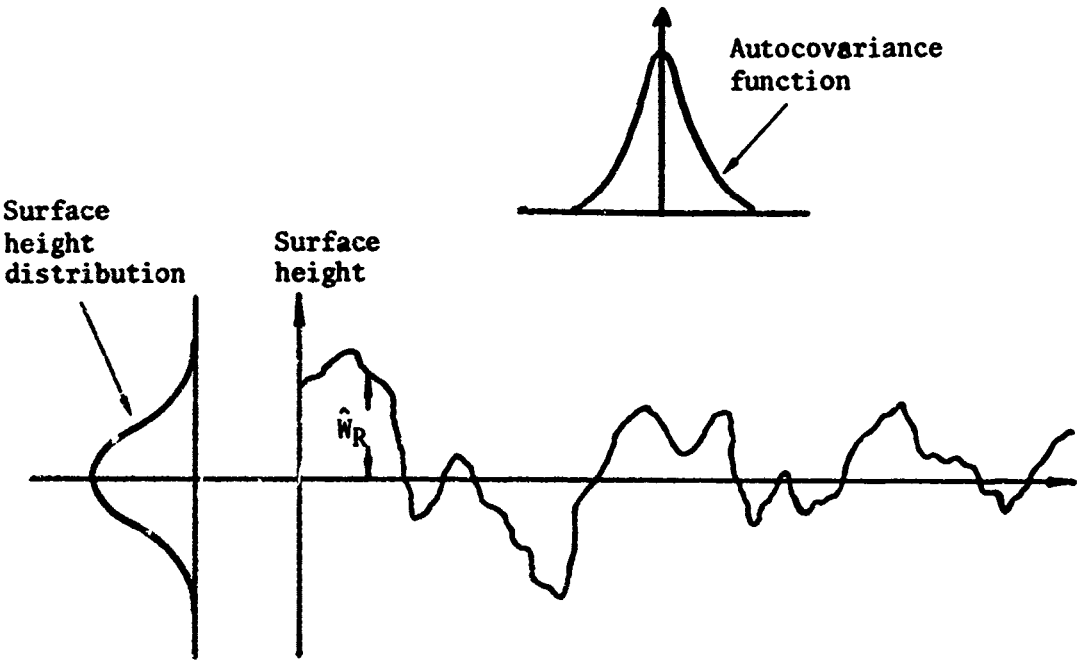

Fig. 10. Illustration of Surface Height Variations and Associated Statistical Parameters.

The random component of the pupil function due to the scattering surface similarly has an amplitude and phase component

$$p_R(\hat{x},\hat{y};0) = \sqrt{R(\hat{x},\hat{y};0)}\, e^{i4\pi\hat{W}_R(\hat{x},\hat{y};0)}, \tag{32a}$$

where R is the reflectance of the scattering surface and $\hat{W}_R$ is the above-mentioned surface height variation. Note that the phase variations on the reflected wavefront are twice as large as the actual variations on the reflecting surface.

Scattered Wave Field on a Hemisphere

The results of the previous chapter, [Eq. (29)], indicate that the complex amplitude distribution on the observation hemisphere is given directly by the Fourier transform of $U_o(\hat{x},\hat{y};0)$

$$U(\alpha,\beta;\hat{r}) = \gamma \frac{e^{i2\pi\hat{r}}}{i\hat{r}} \mathcal{F}\{U_o(\hat{x},\hat{y};0)\}. \tag{33}$$

The total reflected flux P is obtained by applying Rayleigh's theorem from Fourier transform theory

$$P = \iint_{-\infty}^{\infty} \frac{\hat{r}^2}{\gamma^2} |U(\alpha,\beta;\hat{r})|^2 d\alpha d\beta = a_o^2 \iint_{-\infty}^{\infty} |p(\hat{x}',\hat{y}';0)|^2 d\hat{x}' d\hat{y}'. \tag{34}$$

Noting that $d\omega = d\alpha d\beta/\gamma$, the radiant intensity of the scattering system can be written as

$$I(\alpha,\beta) = \frac{dP}{d\omega} = \frac{\hat{r}^2}{\gamma} |U(\alpha,\beta;\hat{r})|^2 = a_o^2 \gamma |\mathcal{F}\{p(\hat{x},\hat{y};0)\}|^2. \tag{35}$$

Utilizing the autocorrelation theorem of Fourier transform theory, this is equivalent to

$$I(\alpha,\beta) = a_o^2 \gamma \mathcal{F}\left\{ \iint_{-\infty}^{\infty} p(\hat{x}',\hat{y}';0) p^*(\hat{x}'-\hat{x},\hat{y}'-\hat{y};0) d\hat{x}' d\hat{y}' \right\}. \tag{35a}$$

The autocorrelation function of a Lambertian surface approaches a Dirac δ-function; hence, its Fourier transform is constant and we obtain

$$I_L(\alpha,\beta) = \gamma K, \quad K = \text{constant} \tag{35b}$$

which is consistent with Lambert's cosine law.

The Effective Transfer Function of a Scattering System

Following the standard procedure used in image evaluation, the effective transfer function of the scattering system is defined as the normalized autocorrelation of the pupil function

$$\mathscr{H}(\hat{x},\hat{y};0) = \frac{\displaystyle\iint_{-\infty}^{\infty} p(\hat{x}',\hat{y}';0)p^*(\hat{x}'-\hat{x},\hat{y}'-\hat{y};0)d\hat{x}'d\hat{y}'}{\displaystyle\iint_{-\infty}^{\infty} |p(\hat{x}',\hat{y}';0)|^2 d\hat{x}'d\hat{y}'} . \tag{36}$$

The effective spread function of the scattering system is now defined in the usual way as the Fourier transform of the transfer function

$$S(\alpha,\beta) = \mathscr{F}\{\mathscr{H}(x,y;0)\} = \frac{\mathscr{F}\left\{\displaystyle\iint_{-\infty}^{\infty} p(\hat{x}',\hat{y}';0)p^*(\hat{x}'-\hat{x},\hat{y}'-\hat{y};0)d\hat{x}'d\hat{y}'\right\}}{\displaystyle\iint_{-\infty}^{\infty} |p(\hat{x}',\hat{y}';0)|^2 d\hat{x}'d\hat{y}'} \tag{37}$$

Direct substitution from Eq. (34) and Eq. (35a) results in the following expression for the effective spread function in terms of the radiant intensity of the scattering system

$$S(\alpha,\beta) = \frac{1}{\gamma P} I(\alpha,\beta). \tag{37a}$$

Scattering from Optical Surfaces

Let the height variations $\hat{W}_R$ of a given illuminated area on a scattering surface be a two-dimensional sample function $\hat{W}_{Ri}(\hat{x},\hat{y};0)$. A

random process, $\hat{W}_R(\hat{x},\hat{y};0)$, is made up of an ensemble of such functions as shown in Fig. 11. For fixed spatial coordinates, $\hat{W}_R(\hat{x}_1,\hat{y}_1;0)$ is a random variable. And, for a specific sample function with fixed spatial coordinates, $\hat{W}_{Ri}(\hat{x}_1,\hat{y}_1;0)$ is a single number.

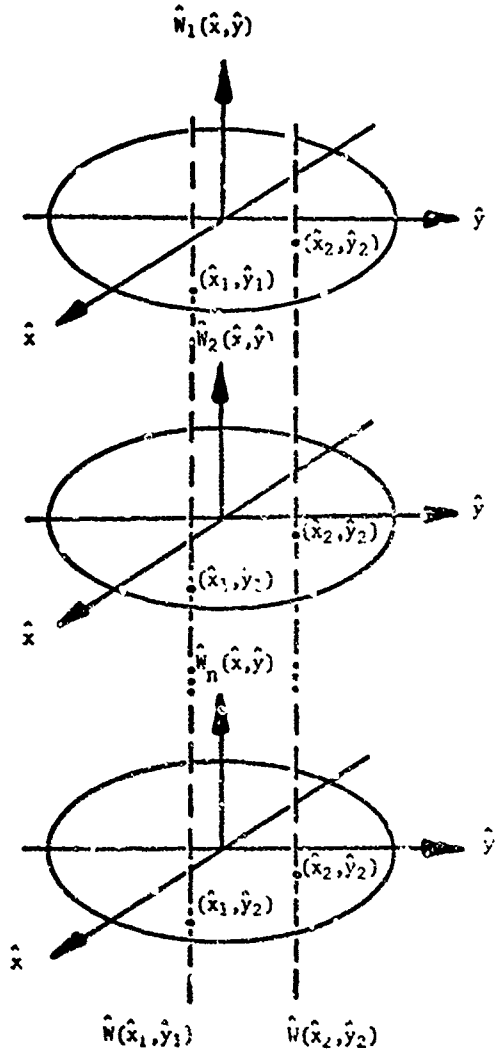

Fig. 11. An Ensemble of Two-Dimensional Sample Functions $\hat{W}_i(\hat{x},\hat{y})$ Representing Surface Height Variations Constitutes a Random Process $\hat{W}(\hat{x},\hat{y})$.

Two random variables, $\hat{W}(\hat{x}_1,\hat{y}_1)$ and $\hat{W}(\hat{x}_2,\hat{y}_2)$ with fixed spatial coordinates are also shown.

Assumptions Concerning the Statistical Properties of an Optical Surface

We are primarily interested in the scattering behavior of optical surfaces. The following assumptions are made concerning the statistical properties of an optical surface prepared by conventional fabrication techniques on ordinary optical materials:

1. The reflectance R is constant over the entire surface. This assumption is not essential but it is reasonable and furthermore it has been shown by Shack (1967) that phase fluctuations will dominate over amplitude fluctuations in their combined effect on the spread function.
2. $\hat{W}_R(\hat{x},\hat{y};0)$ is a single-valued gaussian random process.
3. $\hat{W}_R(\hat{x},\hat{y};0)$ is at least locally stationary in the statistical sense (i.e., surface is homogeneous and isotropic).
4. The random variables $\hat{W}_R(\hat{x}_1,\hat{y}_1;0)$ and $\hat{W}_R(\hat{x}_2,\hat{y}_2;0)$, produced by any two fixed pairs of spatial coordinates, are jointly normal regardless of their correlation coefficient.
5. $\hat{W}_R(\hat{x},\hat{y};0)$ is weakly ergodic (i.e., the mean and autocorrelation function determined by space averages using a single sample function $\hat{W}_{Ri}(\hat{x},\hat{y};0)$ are the same as those determined by ensemble averages).

The Effective Transfer Function of a Scattering Surface

Substituting Eq. (31) into Eq. (36) we obtain

$$\mathcal{H}(\hat{x},\hat{y};0) = \frac{\iint_{-\infty}^{\infty} a_{L1}a_{L2}\, e^{i2\pi[\hat{W}_{L1}-\hat{W}_{L2}]}\, e^{i4\pi[\hat{W}_{R1}-\hat{W}_{R2}]}\, d\hat{x}'d\hat{y}'}{\iint_{-\infty}^{\infty} |a_{L1}|^2\, d\hat{x}'d\hat{y}'} \tag{38}$$

where

$$\begin{aligned} a_{L1} &= a_L(\hat{x}',\hat{y}';0) \\ a_{L2} &= a_L(\hat{x}'-\hat{x},\ \hat{y}'-\hat{y};\ 0) \\ \hat{W}_{L1} &= \hat{W}_L(\hat{x}',\hat{y}';0) \\ \hat{W}_{L2} &= \hat{W}_L(\hat{x}'-\hat{x},\ \hat{y}'-\hat{y};\ 0) \\ \hat{W}_{R1} &= \hat{W}_R(\hat{x}',\hat{y}';0) \\ \hat{W}_{R2} &= \hat{W}_R(\hat{x}'-\hat{x},\ \hat{u}'-y,\ 0). \end{aligned} \tag{39}$$

The above expression for the transfer function contains the random variables W_{R1} and W_{R2}; therefore, taking the expected value we have

$$E\{\mathcal{H}(x,y;0)\} = \frac{\iint_{-\infty}^{\infty} a_{L1}a_{L2}\, e^{i2\pi[\hat{W}_{L1}-\hat{W}_{L2}]}\, E\left\{e^{i4\pi[\hat{W}_{R1}-\hat{W}_{R2}]}\right\} d\hat{x}'d\hat{y}'}{\iint_{-\infty}^{\infty} |a_L|^2 d\hat{x}'d\hat{y}'} \tag{40}$$

Since the random variables involved are assumed to be stationary, the expected value under the integral is independent of $\hat{x}'$ and $\hat{y}'$ and can be taken outside the integral

$$E\{\mathcal{H}(\hat{x},\hat{y};0)\} = E\left\{e^{i4\pi[\hat{W}_{R1}-\hat{W}_{R2}]}\right\} \frac{\iint_{-\infty}^{\infty} a_{L1}a_{L2}e^{i2\pi[\hat{W}_{L1}-\hat{W}_{L2}]}\,d\hat{x}'d\hat{y}'}{\iint_{-\infty}^{\infty} |a_L|^2 d\hat{x}'d\hat{y}'} . \quad (41)$$

We now recognize the normalized autocorrelation function in the above equation to be the transfer function of the optical system producing the incident beam

$$\mathcal{H}_L(\hat{x},\hat{y};0) = \frac{\iint_{-\infty}^{\infty} a_{L1}a_{L2}e^{i2\pi[\hat{W}_{L1}-\hat{W}_{L2}]}\,d\hat{x}'d\hat{y}'}{\iint_{-\infty}^{\infty} |a_L|^2 d\hat{x}'d\hat{y}'} . \quad (42)$$

The average quantity in Eq. (41) is therefore the equivalent transfer function of the scattering surface

$$\mathcal{H}_R(\hat{x},\hat{y};0) = E\left\{e^{i4\pi[\hat{W}_{R1}-\hat{W}_{R2}]}\right\} . \quad (43)$$

But this is merely the joint characteristic function (Papoulis (1965), p. 225) of the two random variables $\hat{W}_{R1}$ and $\hat{W}_{R2}$. Since $\hat{W}_{R1}$ and $\hat{W}_{R2}$ are jointly normal random variables, it can be shown

that (see Papoulis (1965), p. 226))

$$E\left\{e^{i4\pi[\hat{W}_{R1}-\hat{W}_{R2}]}\right\} = e^{i4\pi(\eta_1-\eta_2)}e^{-8\pi^2(\sigma_1^2-2C_{12}+\sigma_2^2)} \tag{44}$$

where

$$C_{12} \equiv E\{(\hat{W}_{R1}-\eta_1)(\hat{W}_{R2}-\eta_2)\} \tag{45}$$

is the covariance function of the random variables $\hat{W}_{R1}$ and $\hat{W}_{R2}$. But $\hat{W}_{R1}$ and $\hat{W}_{R2}$ are identical functions merely displaced from one another; hence

$$\sigma_1 = \sigma_2 = \sigma_{\hat{W}}, \qquad \eta_1 = \eta_2 \tag{46}$$

and

$$C_{12} \equiv C_{\hat{W}}(\hat{x},\hat{y}) \equiv \text{autocovariance of } \hat{W}_R. \tag{47}$$

The equivalent transfer function of the scattering surface is thus given by

$$\mathscr{K}_R(\hat{x},\hat{y};0) = e^{-(4\pi\sigma_{\hat{W}})^2\left[1-\frac{C_{\hat{W}}(\hat{x},\hat{y})}{\sigma_{\hat{W}}^2}\right]} \tag{48}$$

where $\sigma_{\hat{W}}^2$ is the variance of the surface height distribution function and $C_{\hat{W}}(\hat{x},\hat{y})$ is the two-dimensional autocovariance function of the surface.

Considerable insight into the scattering process can now be obtained by considering the nature of this transfer function. The autocovariance function approaches the value $\sigma_{\hat{W}}^2$ as the displacement

approaches zero. The equivalent transfer function thus approaches unity as expected. As the displacement approaches infinity the autocovariance function approaches zero and the equivalent transfer function approaches a plateau of height $\exp[-(2\pi\sigma_{\hat{W}})^2]$.

The equivalent transfer function of the scattering surface can thus be regarded as the sum of a constant component and a bell-shaped component as shown in Fig. 12a. Equation (48) can therefore be rewritten as

$$\mathcal{H}_R(\hat{x},\hat{y};0) = A + B\,Q(\hat{x},\hat{y};0), \tag{49}$$

where

$$A = e^{-(4\pi\sigma_{\hat{W}})^2}$$

$$B = 1 - e^{-(4\pi\sigma_{\hat{W}})^2}$$

$$Q(\hat{x},\hat{y};0) = \frac{e^{(4\pi\sigma_{\hat{W}})^2 \frac{C_{\hat{W}}(\hat{x},\hat{y})}{\sigma_{\hat{W}}^2}} - 1}{e^{(4\pi\sigma_{\hat{W}})^2} - 1}. \tag{50}$$

The Effective Spread Function of a Scattering Surface

The significance of this interpretation of the equivalent transfer function of the scattering surface is dramatically shown by the inferred properties of the corresponding spread function. Since the

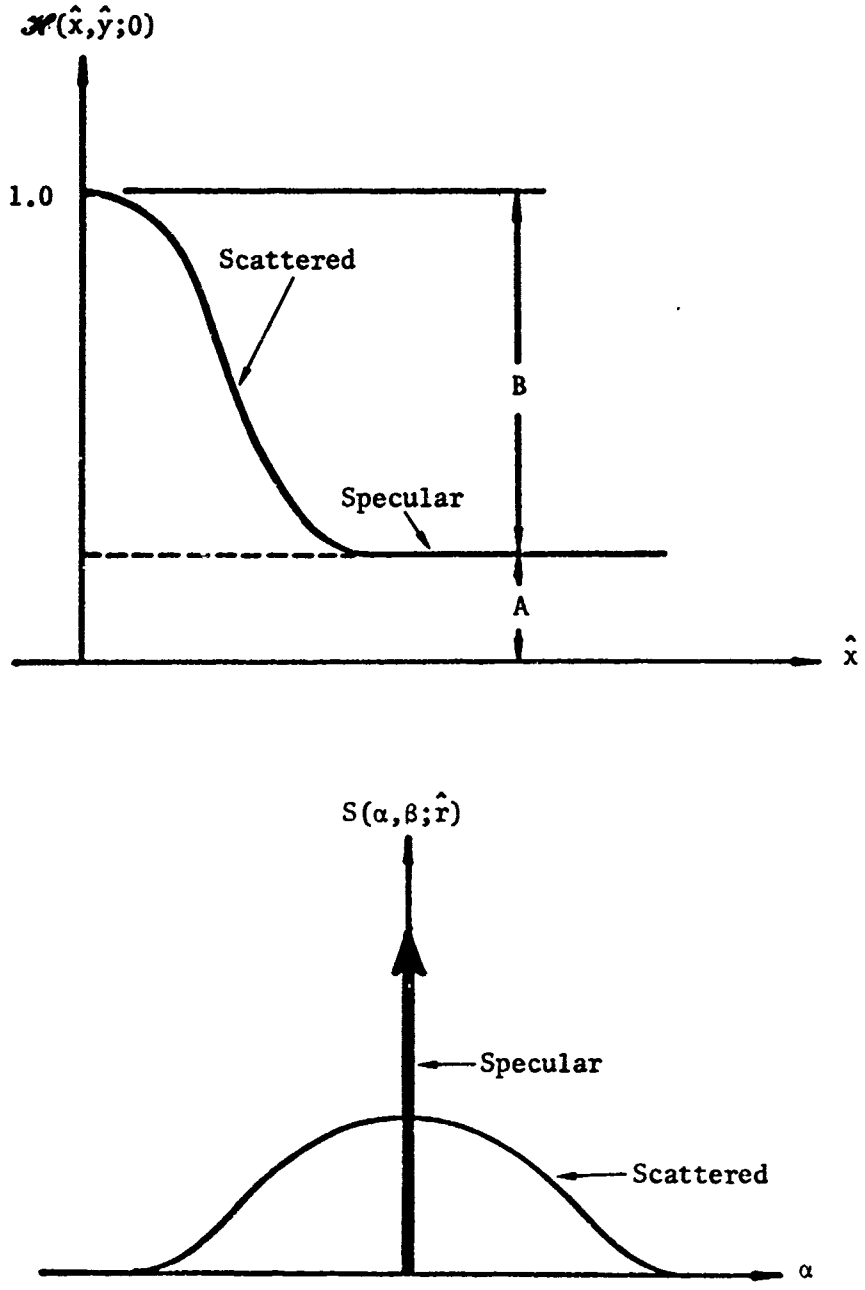

Fig. 12. (a) Effective Transfer Function of a Scattering Surface.
(b) Spread Function Associated with a Scattering Surface.

transfer function is the sum of two separate components, the equivalent spread function of the scattering surface is the sum of the inverse Fourier transforms of the two component functions. The constant component transforms into a delta function, and the bell-shaped component transforms into another bell-shaped function as shown in Fig. 12b. Hence the scattering surface reflects an incident beam of light as a specularly-reflected beam of diminished intensity surrounded by a halo of scattered light. Furthermore, the relative power distribution between the specular component and the scattered component of the effective spread function are given by the quantities A and B respectively.

Note that as more and more light is scattered, energy is transferred from the specular component of the spread function into the scattered component of the spread function. For a perfectly Lambertian reflector the specular component disappears completely from the spread function.

Relationship between the Spread Function and the BRDF

From the above analysis it is clear that the Bidirectional Reflectance Distribution Function (BRDF), (see Appendix C), which is appearing frequently in the radiometry literature, is merely an infinite family of two-dimensional spread functions.

In general, the above scattering function (or the BRDF of diffuse reflectance measurements) will change with angle of incidence just

as the point spread function of an optical imaging system will, in general, vary with the field position of the point source. However, the analysis of imaging systems is greatly simplified by assuming an isoplanatic system in which the point spread function does not change with field position (and this is a reasonable assumption for many practical imaging systems). Similarly, the analysis of light scattering systems will be greatly simplified if they can be shown to be shift-invariant (i.e., if the shape of the scattering function does not change with the angle of incidence). If this is true, the four-dimensional BRDF degenerates into a single two-dimensional spread function.

Shift Invariance in Direction Cosine Space

The scattered light distribution on an observation hemisphere will appear to consist of the sum of two components, a core which is the delta function convolved with the spread function of the optical system producing the incident beam, and a scattering function which is the bell-shaped halo convolved with the spread function of the optical system.

In Fig. 13 we have merely replaced the diffracting aperture of Fig. 8 with a scattering surface and the geometry of the measurements has been folded about the reflecting plane. Hence, we have the incident beam striking the scattering surface at some angle of incidence, a specularly-reflected beam striking the observation hemisphere, and the scattered light distribution being sampled at an arbitrary point with

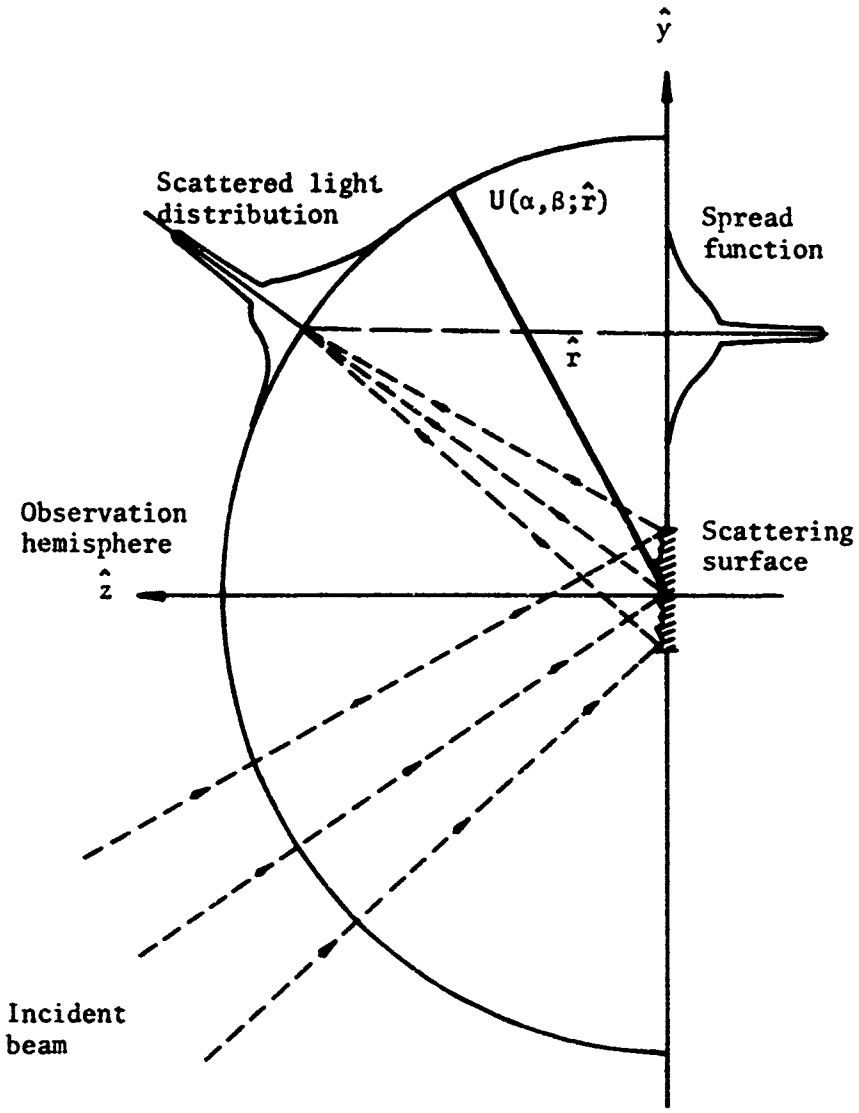

Fig. 13. Geometrical Relationship Between Incident Beam, Scattering Surface, the Measured Scattered Light Distribution, and the Resulting Spread Function.

direction cosine coordinates α and β. The scattered light distribution on the hemisphere will, in general, change shape drastically with angle of incidence--becoming quite skewed and asymmetrical at large angles of incidence. However, our theory predicts that, for certain surfaces with well-behaved statistics, if the data collected on the hemisphere is plotted as a function of the direction cosines of the position vector of the observation point, this new scattering function will not change shape but will merely be shifted in direction cosine space with changes in angle of incidence. This is a rather significant development which has profound implications regarding the quantity of data required to completely characterize a scattering surface. However, it remains to be shown whether scattering surfaces of practical interest can experimentally be shown to obey these predictions.

CHAPTER IV

SURFACE SCATTER MEASUREMENTS

Apparatus

An instrument has been designed and built at the Optical Sciences Center for making scattered light measurements on a hemisphere as described in the previous chapter. A schematic diagram of this apparatus is shown in Fig. 14. The incident light passes through a chopper so that synchronous detection with a PAR lock-in amplifier can be made. The mechanical apparatus shown in Fig. 15 is located in a small photometric darkroom in which the experiment is conducted. A movable arm with folding mirrors can be positioned to direct the incident beam onto the sample at any desired angle. A lens positioned on this arm focuses the incident radiation onto the hemisphere mapped out by the detector; hence, the geometrical configuration is consistent with that illustrated in Fig. 13 of the previous chapter. Two separate driving mechanisms allow us to measure the scattered light distribution over the entire hemisphere bounded by the plane of the sample.

The Light Source

The light source employed is a Spectra-Physics Model 165 Argon Ion Laser. The laser is operated with a light-regulated, single-frequency output which assures intensity regulation to within

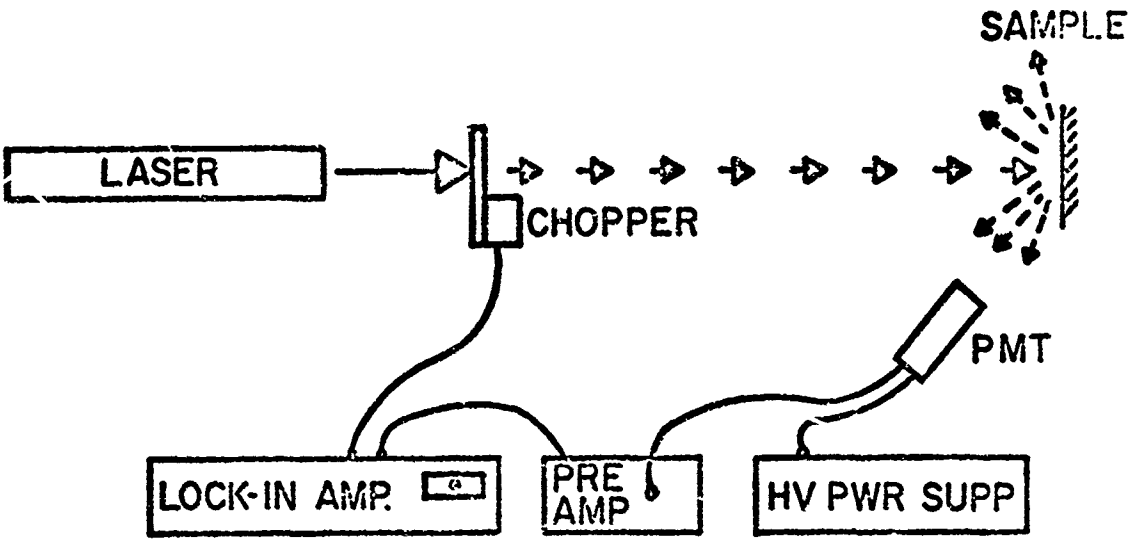

Fig. 14. Schematic Diagram of Scatter Measurement Apparatus.

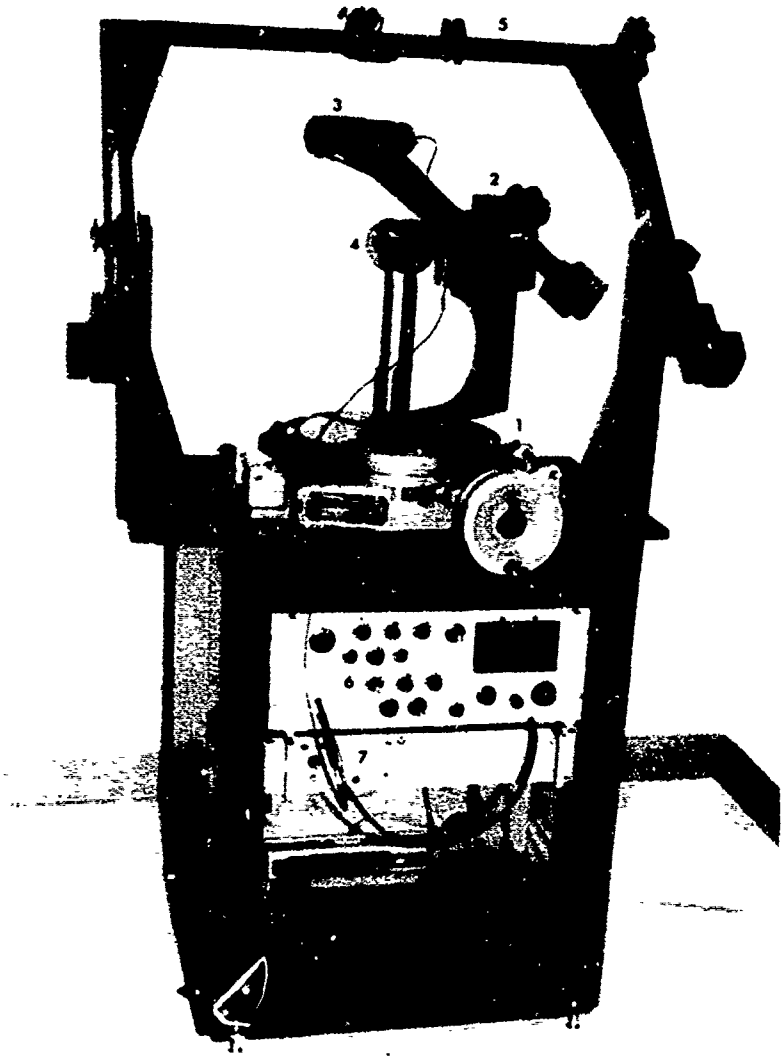

Fig. 15. Apparatus for Measuring Scattered Light Distribution from Optical Surfaces.

(1) Precision rotary table, (2) worm gear drive for arm supporting detector, (3) photomultiplier tube and fiber-optic probe, (4) sample holder, (5) movable arm with folding mirrors and lens for directing and focusing incident beam, (6) P.A.R. lock-in amplifier, (7) high voltage power supply for PMT.

one percent. The measurements were made with approximately 20 mw of power in the incident beam at a wavelength of 0.5145 μm.

The Detector Unit

The detector is a Phillips one-inch, end-on photomultiplier having an S-20 photocathode. Light reaches the photomultiplier by way of a rigid fiber-optic probe. Such a probe offers several distinct advantages in light sampling. In addition to allowing increased angular resolution throughout the sampling space, and enabling us to sample within half a degree of the incident or specularly-reflected beams, it provides the ability to control the field of view of the detector for the purpose of stray light rejection.

The original configuration consisted of a rigid fiber-optic bundle bent such that one end was pointed toward the illuminated spot on the sample. This end of the bundle thus acted as the collecting aperture for the detection system. The other end of the fiber-optic bundle protruded into the photomultiplier tube housing followed by a series of baffles to limit the field of view of the detector as shown in Fig. 16a. This resulted in a detector response which had a gaussian dependence upon field angle.

However, by introducing a small collecting lens and a field stop in front of the fiber-optic bundle as shown in Fig. 16b, the baffles can be eliminated and a well-defined field of view of any desired size can be obtained by properly choosing the size of the field stop. This is

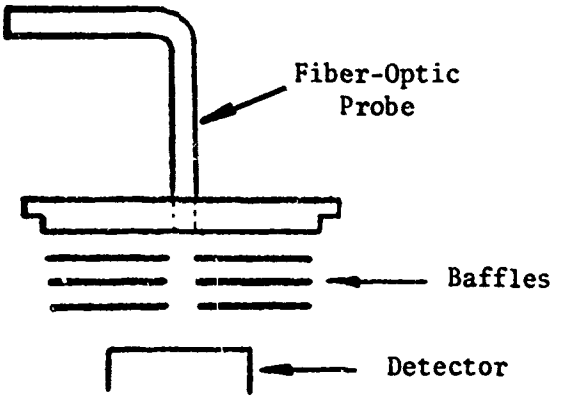

(a)

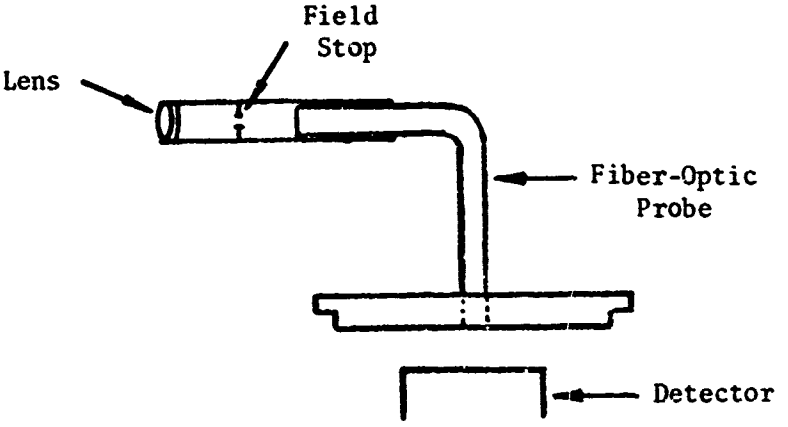

(b)

Fig. 16. (a) Previous Configuration of Detector Probe Unit.
(b) New Configuration of Detector Probe Unit.

more clearly illustrated in Fig. 17. A coated doublet with a 10-mm focal length was edged down and mounted in a black anodized brass tube 3 mm in diameter. A field stop allowing a 5-degree field of view was fabricated and inserted into the tube at the rear focal plane of the lens. This assembly was then positioned onto the end of the fiber-optic bundle. The detector response from a small (point source) light source was then recorded as a function of field angle for both detector probe configurations. The results are displayed for comparison in Fig. 18. Both the flat response and the sharp cutoff obtained with the modified unit are highly desirable features. The flat response promises to eliminate signal variations due to slight misalignment or wobble in the mechanical instrument while scanning over the hemisphere. The ability to keep the field of view small with a very sharp cutoff is essential for stray light rejection.

The scattered light flux from a polished surface varies by several orders of magnitude over the angular range to be measured. Hence the linearity of the PMT was measured using a calibrated neutral density wedge and several known neutral density filters to vary the incident flux. The resulting linearity curve is shown in Fig. 19 and indicates a deviation of less than 1% over a range of five orders of magnitude of the incident flux.

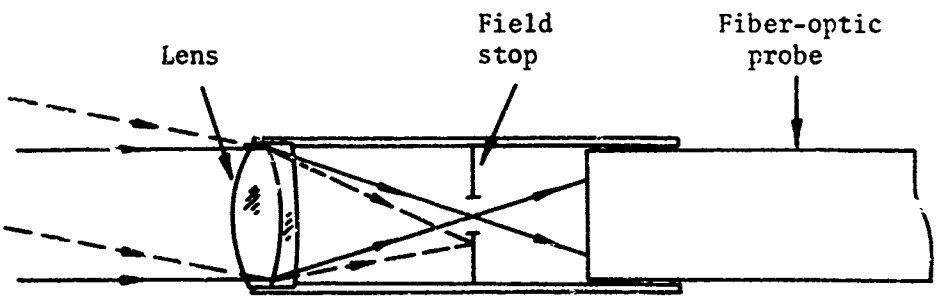

Fig. 17. Detailed Illustration of New Fiber-Optic Probe.

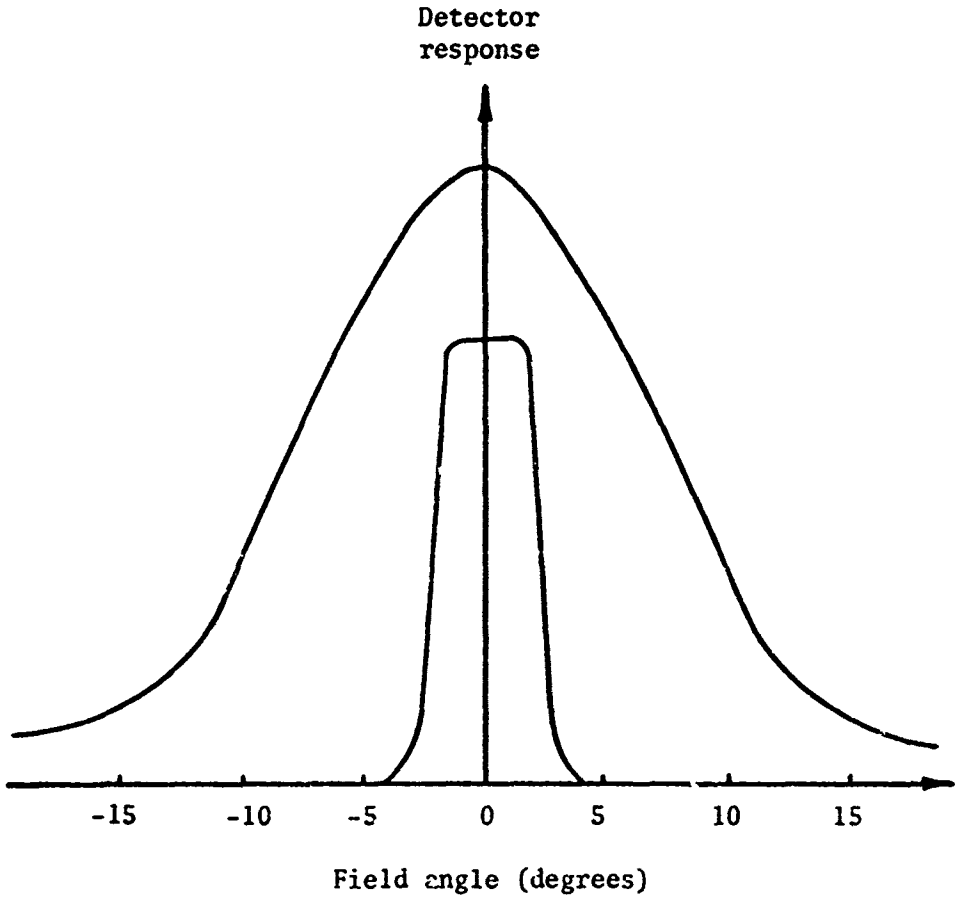

Fig. 18. Detector Response as a Function of Field Angle for Detector Configurations shown in Fig. 16.

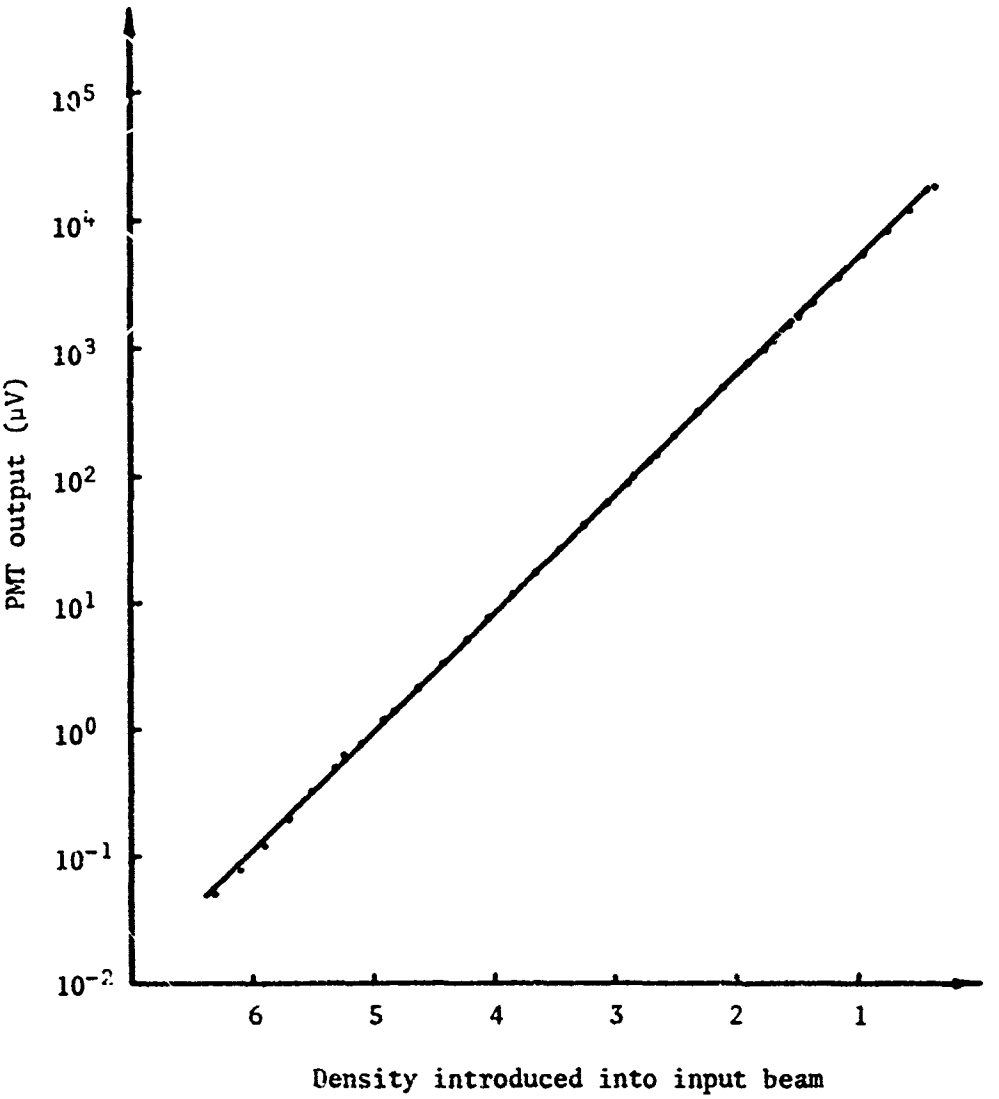

Fig. 19. Photomultiplier Tube Linearity Curve.

The Scanning Mechanism

The mechanical apparatus for measuring the angular distribution of light scattered from optical surfaces was shown in Fig. 15. The detector probe unit is mounted on a rigid arm that can be rotated in either of two orthogonal directions. Rotation about a vertical axis is accomplished by means of a massive precision rotary table. The rigid arm is attached to the rotary table by means of a worm gear arrangement that allows rotation about the horizontal axis. The intersection of these two axes defines the sample location.

The Incident Beam

A large movable arm with appropriate folding mirrors is used to direct the incident beam onto the sample at any desired angle of incidence. Immediately following the last folding mirror the beam is focused onto a pinhole which acts as a spatial filter as shown in Fig. 20. Lens L2 then forms an image of the pinhole upon the hemisphere mapped out by the collecting aperture of the scanning fiber-optic probe. This spatial filter assembly eliminates from the beam incident upon the sample any light scattered from the folding mirrors as well as any diffraction effects from the chopper blade.

Experimental Procedures

The instrument described in the previous section allows us to measure the scattered light distribution over the entire hemisphere bounded by the plane of the sample for all angles of incidence. However,

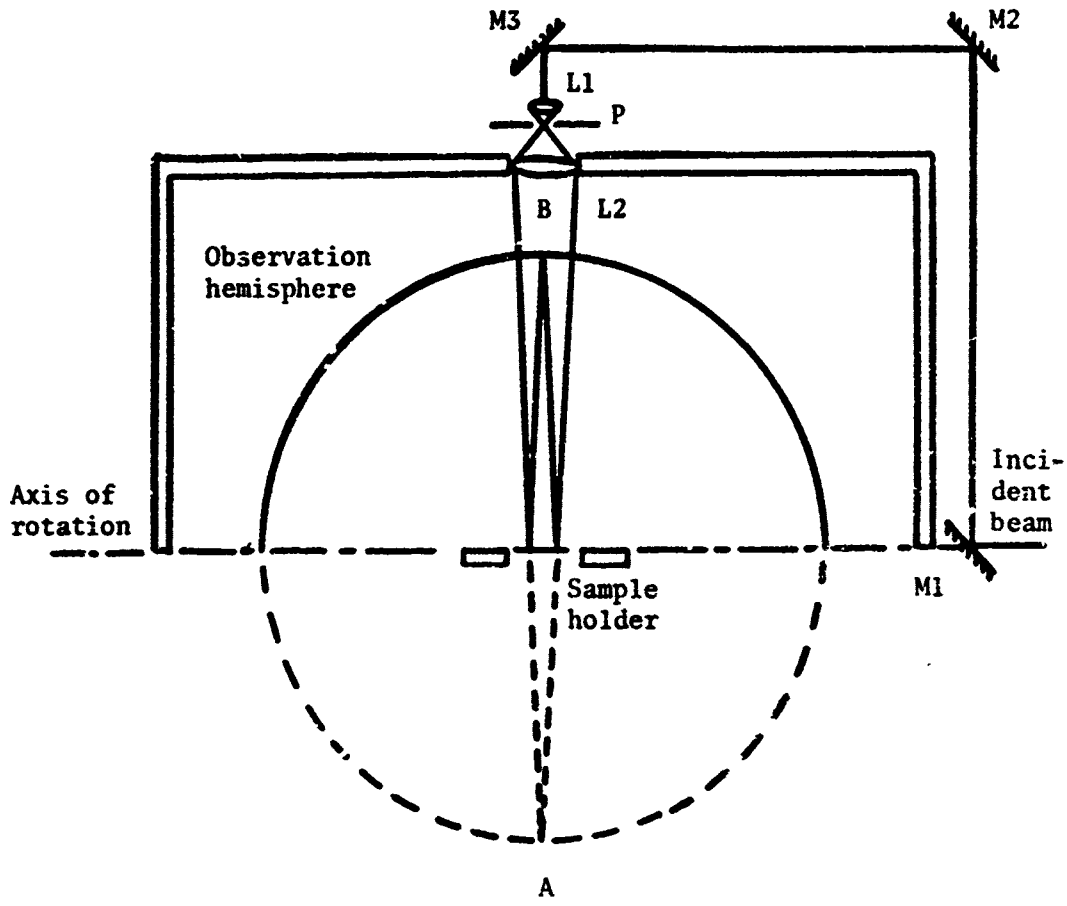

Fig. 20. Detailed Illustration of Movable Arm Supporting the Optical System Forming Incident Beam.

in order to limit the quantity of data to be collected, the scattered radiation field will be sampled in two principal directions. These include the entire plane of incidence and a plane containing the intersection of the specular beam with the unit hemisphere, which is perpendicular to both the plane of incidence and the plane of the sample being tested (see Fig. 21). This particular sampling procedure was chosen because each sampling direction then involves one fixed coordinate in direction cosine space as discussed in the theory section of this report. Furthermore, the apparatus was designed such that each of the two independent drive mechanisms corresponds directly to a given coordinate in direction cosine space. Hence for a given observation point determined by the angles θ and ϕ displayed on the apparatus, the corresponding coordinates in direction cosine space are given by

$$\alpha = \cos\theta \sin\phi$$

$$\beta = \sin\theta. \tag{51}$$

Measurements will be made to within one degree of the specular beam in both directions. These measurements will be made for a variety of angles of incidence on a set of samples consisting of an assortment of glass types having been polished to varying degrees of surface roughness. A sample with a diffuse MgO coating will be used as a reference. Asymmetries that arise as a result of polishing techniques, cleaning, and coating anomalies, can be investigated by rotating the sample about a normal to the surface.

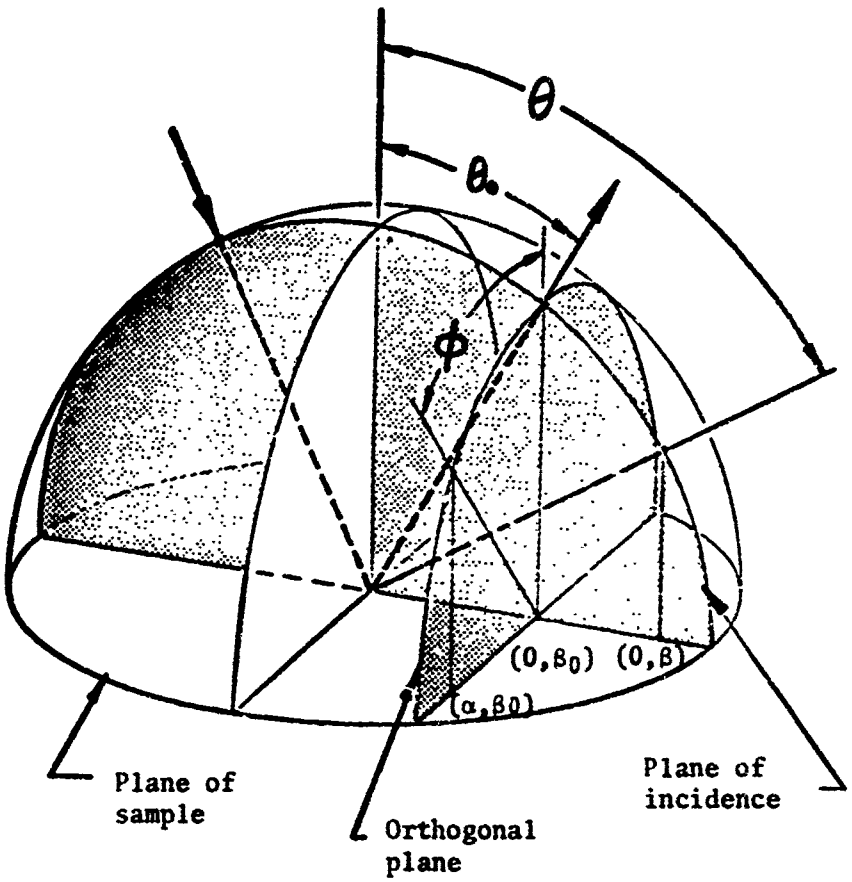

Fig. 21. Geometrical Configuration of Two Principal Planes in which the Scattered Light Field Will Be Sampled.

Sample Preparation

An original goal of the research reported here was to examine the scattering properties of samples whose surface characteristics span those typically produced with optical fabrication techniques.

Surface preparation techniques used to produce a set of samples are outlined in Table 2. All samples were finished to be nominally flat.

The prepared samples were cleaned prior to coating with aluminum. Cleaning consisted of careful washing with Liquinox, a mild detergent, under very warm, filtered tap water. Samples were then mounted in a sample holder while held in distilled water. Once in a holder, samples were moved to an ultrasonic cleaner filled with distilled water for rinsing. Once rinsed the samples were set to dry in a dust-free atmosphere. Dry samples were removed from the sample holders and placed in individual boxes being supported by the edge of their backside. Mott (1971) used a similar cleaning technique, which he describes more completely.

Cleaned dry samples were then placed in a high vacuum chamber and coated to near opacity with pure aluminum. Coating technique varied from the standard only in that excessive care was taken to allow the chamber to reach a pressure below 2×10^{-6} torr prior to coating. The samples were allowed to cool to room temperature prior to removal from the chamber. Each coating run contained ten different samples. Once coated, samples were returned to their individual storage boxes. After all samples were coated, the best samples of each type were selected for

Table 2. Surface Preparation Techniques

No. of Substrate	Set #	Substrate Material	Lap Material	Polishing Medium	Polishing Time	Force Applied Kg/cm
151-153-154-166-165-164-163	1-2	Quartz	Optical Pitch	CeO* (milled 2000 hr.)	8 hr.	0.2
151-153-154-166-165-164-163	1-2	Quartz	Optical Pitch	Distilled H_2O w/same lap	8 hr.	0.2
163-164-165-166	2	Quartz	Optical Pitch	Distilled H_2O w/same lap	12 hr.	0.2
167-168-170-172-174-175-176	4-5	Quartz	Cast Iron	Al_2O_3 (2-μm diam.)	20 min.	0.15
172-174-175-176	5	Quartz	Plate Glass	Al_2O_3 (1-μm diam.)	1 hr.	0.12
219-213-203-200-198-196-194	6-7	Quartz	Cast Iron	Al_2O_3 (30-μm diam.)	20 min.	0.15
200-198-196-194	7	Quartz	Optical Pitch	CeO (milled 500 hr.)	4 hr.	0.12
192-190-188-186-184-180-178	3-10	Quartz	Optical Pitch	CeO (milled 500 hr.)	4 hr.	0.12
186-184-180-178	10	Quartz	Optical Pitch	Al_2O_3 (2-μm diam.)	1 min.	0.12
10-8-7-6-5-3-2	8-9	EDF 3	Optical Pitch	CeO (milled 500 hr.)	4 hr.	0.12
6-5-3-2	9	EDF 3	Optical Pitch	CeO (milled 2000 hr.)	4 hr.	0.12
6-5-3-2	9	EDF 3	Optical Pitch	Distilled H_2O	8 hr.	0.12

*Closed circulation system.

measurement. This selection was made on the basis of individual inspection of each sample while held under a microscope illuminator in an otherwise dark room. Samples that had coating nonuniformities, sleeks or pinholes were rejected as were those with waterspots, large scratches, or otherwise questionable appearance. Prior to each set of scatter measurements, samples were again individually inspected for flaws. Dust was removed using a commercially available pressurized air can. After the scattering characteristics of each sample were measured, the sample was returned to its individual box.

System Alignment

Prior to making any meaningful scatter measurements it was necessary to systematically align the entire system.

The incident laser beam was first made accurately horizontal. Then the mechanical apparatus was positioned such that the axis of rotation of the movable arm supporting the folding mirrors (see Fig. 20) was colinear with the incident beam. This was accomplished by means of four massive leveling screws at the base of the stand supporting the entire apparatus.

With mirror M1 removed the laser beam passes through the small hole in the center of the bearings upon which the movable arm rotates. This assures that the incident beam is indeed colinear with the axis of rotation and furthermore allows the sample holder, which is mounted on a shaft passing through the axis of the precision rotary table, to be

accurately positioned so that the center of the scattering surface lies at the intersection of these two perpendicular axes.

Mirror M1 is then put into place and adjusted until the laser beam is centered upon mirror M2. Similarly, M2 is adjusted until the beam is centered upon M3.

With the lenses L1 and L2 and the pinhole P removed from the system, mirror M3 is adjusted until the beam is centered upon the sample holder.

The incident beam is then made accurately perpendicular to the axis of rotation of the movable arm by the following procedure. With the sample removed, the rotary table is positioned so that the beam is centered on the detector at position A. A polished sample is placed in the holder and adjusted until the specularly-relfected beam returns precisely along the incident beam. Now the table is rotated until the detector is centered upon the reflected beam at position B. If A and B are not precisely 180° apart, systematically adjust mirrors M2 and M3 and repeat the above procedure.

Lenses L1 and L2 are then placed in the beam and properly centered. And finally, the pinhole P is accurately positioned at the back focal position of lens L1.

With the system properly aligned, the movable arm can be rotated to direct the incident beam at any desired angle without requiring other adjustments to keep the beam centered upon the sample.

An additional requirement is that the PMT with its associated fiber-optic probe be positioned and aligned such that the field of view of the PMT remain accurately centered on the illuminated portion of the sample throughout the entire range of its scanning motion. Provisions were therefore made to allow three degrees of freedom (one translation and two rotation) in adjusting the position and orientation of the PMT housing. Removing the PMT from its housing and illuminating the fiber-optic probe from the back side greatly facilitates this alignment procedure as it allows one to directly observe the field of view on the sample holder while making the necessary adjustments.

Measurement Technique

The sample to be measured is placed in the holder and the movable arm positioned to achieve the desired angle of incidence. A calibrated attenuator is then placed in the incident beam and the detector centered on the specularly-reflected beam. The collecting aperture of the fiber-optic probe is large enough to collect the entire specular beam; hence, the output signal, V_s, of the PMT in this position is proportional to the total flux in the specular beam.

The detector is then moved a known angular distance (approximately one degree) from the specular beam and the attenuator removed. A profile of the scattered light distribution is then measured by scanning the observation hemisphere with the fiber-optic probe. Approximately 30 separate readings are taken at different angular positions between

the specular beam and the plane of the sample. This set of readings is the raw data.

The sample is then removed and the incident beam allowed to pass unobstructed through the sample holder and into a black absorbing Rayleigh's horn. Background measurements are then made along the same profile as above and subtracted from the raw data. These background measurements were found to be completely negligible in most instances.

The data now describes the spread function of the scattering system, which is made up of the spread function of the scattering surface convolved with the spread function of the optical system producing the incident beam. These are shown in Fig. 22.

The spread function of the incident beam is then measured by again placing the calibrated attenuator in the incident beam and centering the detector on the direct beam passing through the empty sample holder. Since the collecting aperture of the fiber-optic probe is large enough to collect most of the incident beam, the output signal, V_o, of the PMT in this position represents a good approximation to the total flux in the incident beam. The detector is then moved a known angular distance (approximately one degree) from the direct beam and the attenuator removed. A profile of the incident beam is then measured. These readings rapidly diminish to zero within five degrees of the peak value.

Since the spread function of the incident beam (Fig. 22a) is narrow compared to the scattering function of the surface (Fig. 22b), the scattering portion of the surface spread function is virtually

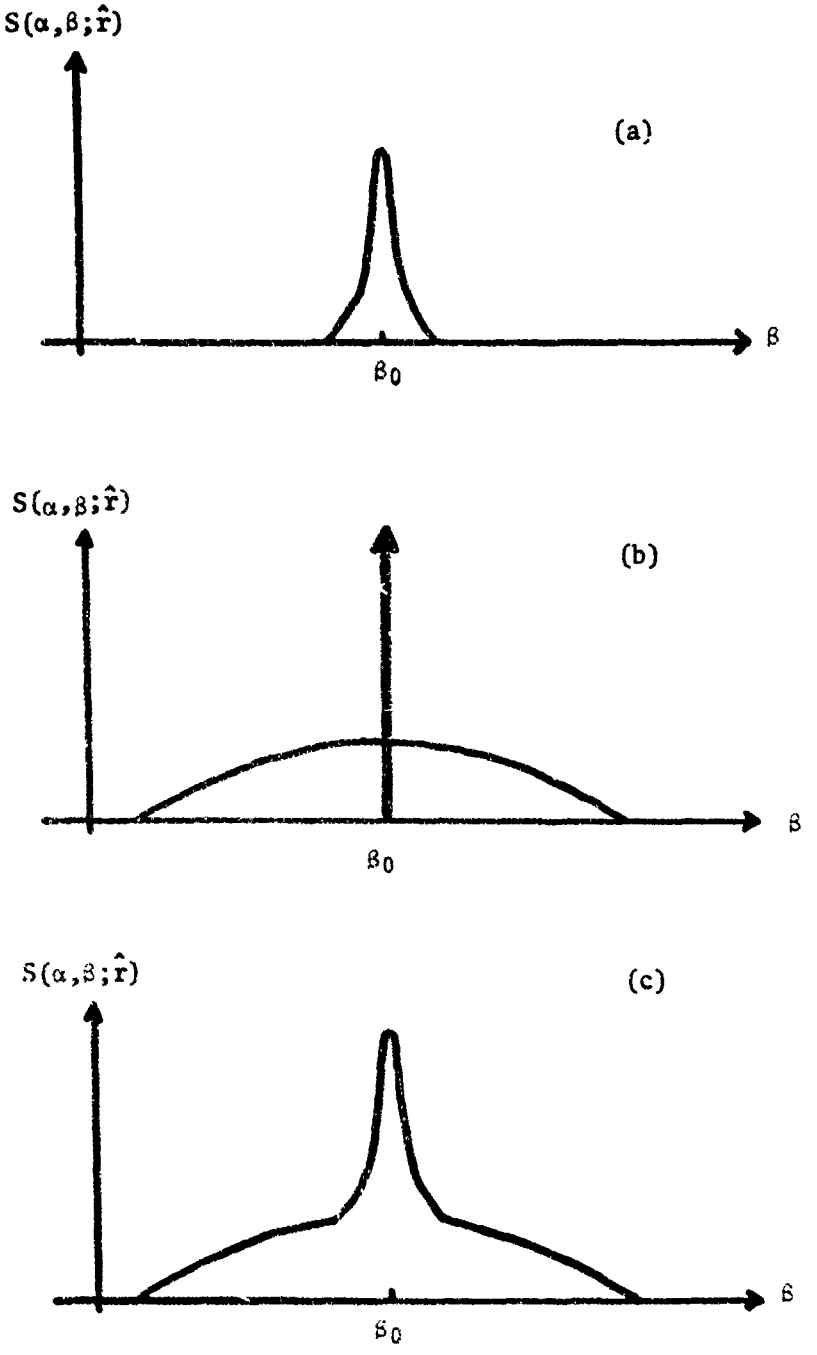

Fig. 22. (a) Spread Function of Incident Beam.
(b) Spread Function of Scattering Surface.
(c) Spread Function of Scattering System.

unchanged by the convolution operation while the delta function component merely replicates the beam spread function. The desired scattering function can thus be obtained by subtracting the beam spread functi n readings from the raw data.

Data and Results

Rather extensive scatter measurements have been made on two representative surfaces. One is a ground glass surface which is a very diffuse reflector. The other is an optically polished surface which is a nice specular reflector. Both samples were coated with aluminum prior to making the measurements. Four separate scattering profiles from the specular beam to the plane of the sample (see Fig. 21) were made at several angles of incidence.

The backscattering profile of the scattered light distribution for these two samples is shown in Fig. 23 for several different angles of incidence. Note that we are plotting the quantity $V/V_{O\gamma}$ along the ordinate. Since V is proportional to the power collected per unit solid angle subtended by the fiber-optic probe and V_O is proportional to the total power in the incident beam, we can write

$$\frac{V}{V_{O\gamma}} = \frac{P/\Delta\omega}{P_{O\gamma}} = \frac{P/(A_\gamma \Delta\omega)}{P_O/A} = \frac{L_r(\theta_i, \phi_i;\ \theta_r, \phi_r)}{E_i(\theta_i, \phi_i)} \tag{52}$$

where A is the illuminated area on the sample.

Hence the quantity plotted along the ordinate is equivalent to the reflected radiance in the sampled direction divided by the incident

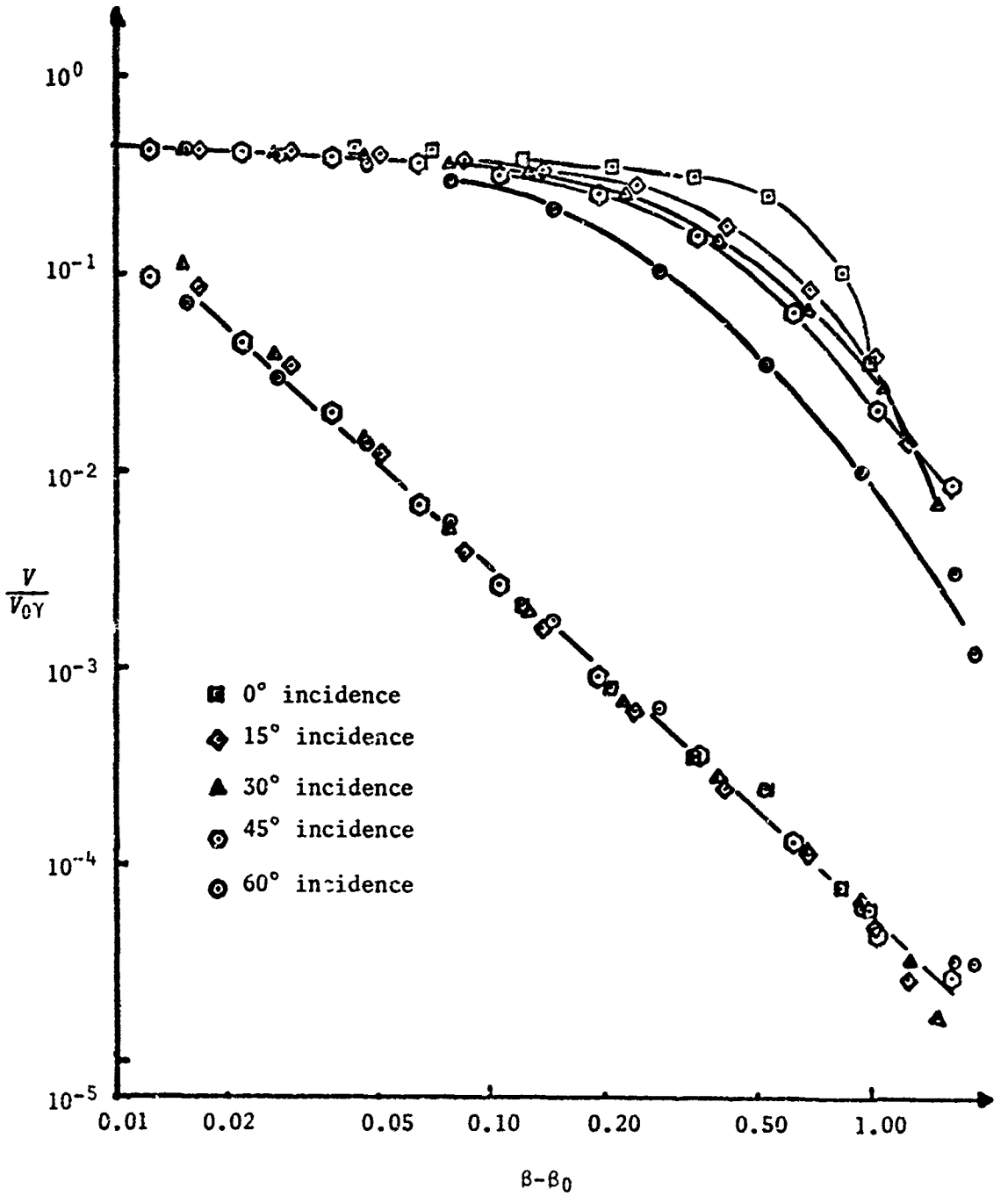

Fig. 23. Comparison of Scatter Profiles for Different Incident Angles.

irradiance, which is precisely the way the BRDF is defined. Our scattering curves are therefore one-dimensional profiles of the four-dimensional BRDF. Also, in accordance with our theory we are plotting this function versus the quantity $\beta-\nu_0$, which is the distance of the observation point from the specular beam in direction cosine space. Both coordinates are then plotted on a logrithmic scale. For the polished sample, the five curves with the incident angle varying from zero to 60° coincide almost perfectly. Hence, it is apparent that the scattering function does not appreciably change with the angle of incidence. The corresponding curves for the rough sample coincide for a substantial range of angles then begin to depart somewhat at the large angles.

The four separate profiles of the scattered light distribution from the same two samples with the incident beam at 45° are shown in Fig. 24. Again the curves for the polished sample coincide almost perfectly, suggesting a rotationally-symmetric distribution in direction cosine space. Some asymmetry is noted in the scattered light distribution from the rough sample.

The data on Figs. 23 and 24 confirm that for a certain class of surfaces (in which optically polished glass is definitely a member, and ground glass can perhaps be included to a lesser extent), the scattering properties are indeed shift invariant, and can be completely characterized by a single set of measurements at a fixed angle of incidence!

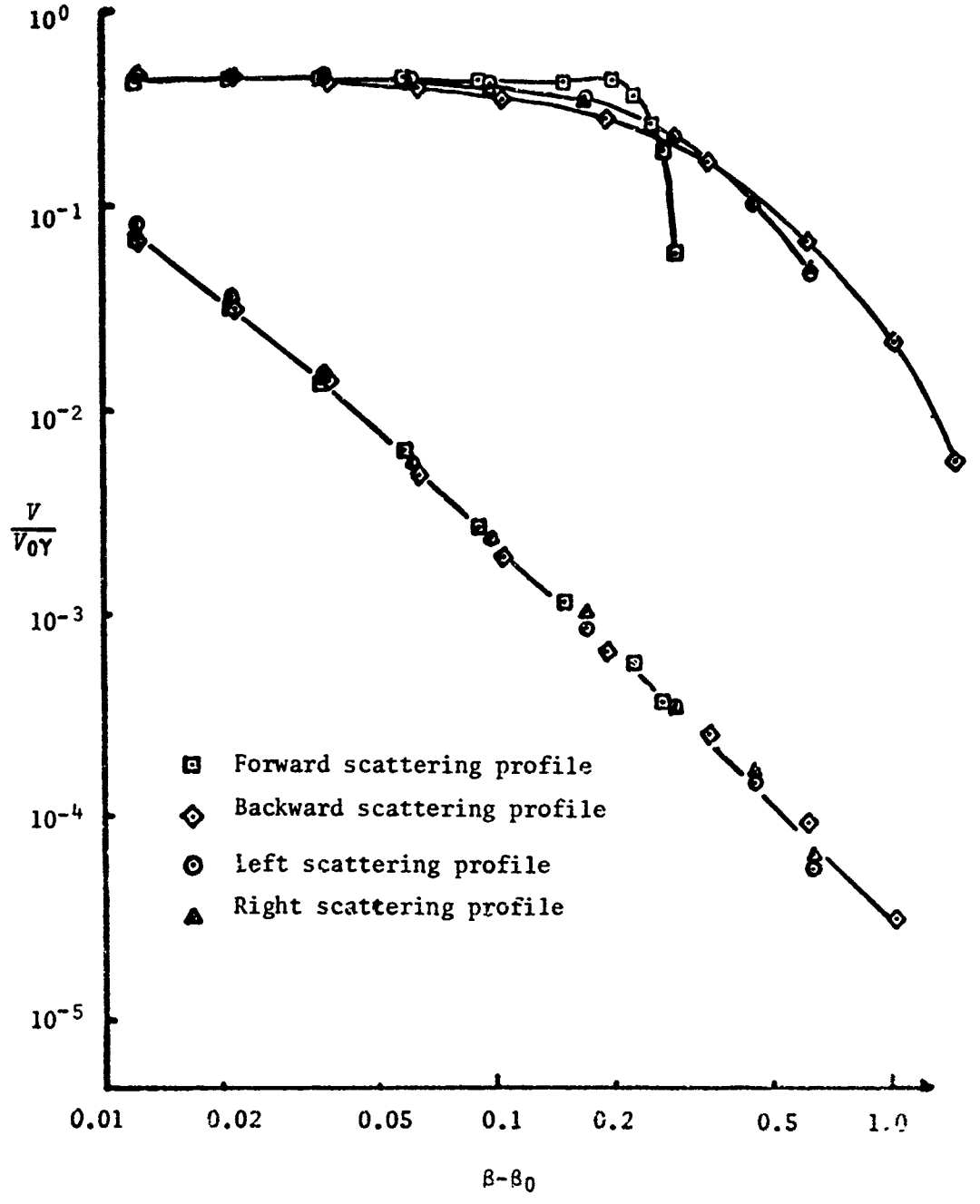

Fig. 24. Comparison of Scatter Profiles Taken in Different Directions for an Incident Beam at 45 Degrees.

The scattering function for a variety of samples with a wide range of rms surface roughnesses are exhibited in Fig. 25. Note that the MgO surface, which is somewhat of a diffuse reflectance standard, yields a straight horizontal line as a Lambertain reflector should. Since the radiance of a Lambertian source is given by [Hudson (1969)]

$$L = \frac{M}{\pi} \tag{53}$$

where M is the total emittance into a hemisphere, the height of the MgO scattering curve is taken to be $1/\pi$ and all other scatter measurements are normalized accordingly. The values of the rms surface roughness are merely estimates.

It may be of interest to compare the scattering curves resulting from special materials or unusual fabrication techniques with those of more conventional optical surfaces. For example, the result of scattering measurements on a polished beryllium sample and an ionically-polished fused quartz sample are shown in Fig. 26 along with some curves from conventional optical surfaces. All measurements are normalized by the reflectance of the surface so that the beryllium does not appear to have better scattering characteristics due to its lower reflectance.

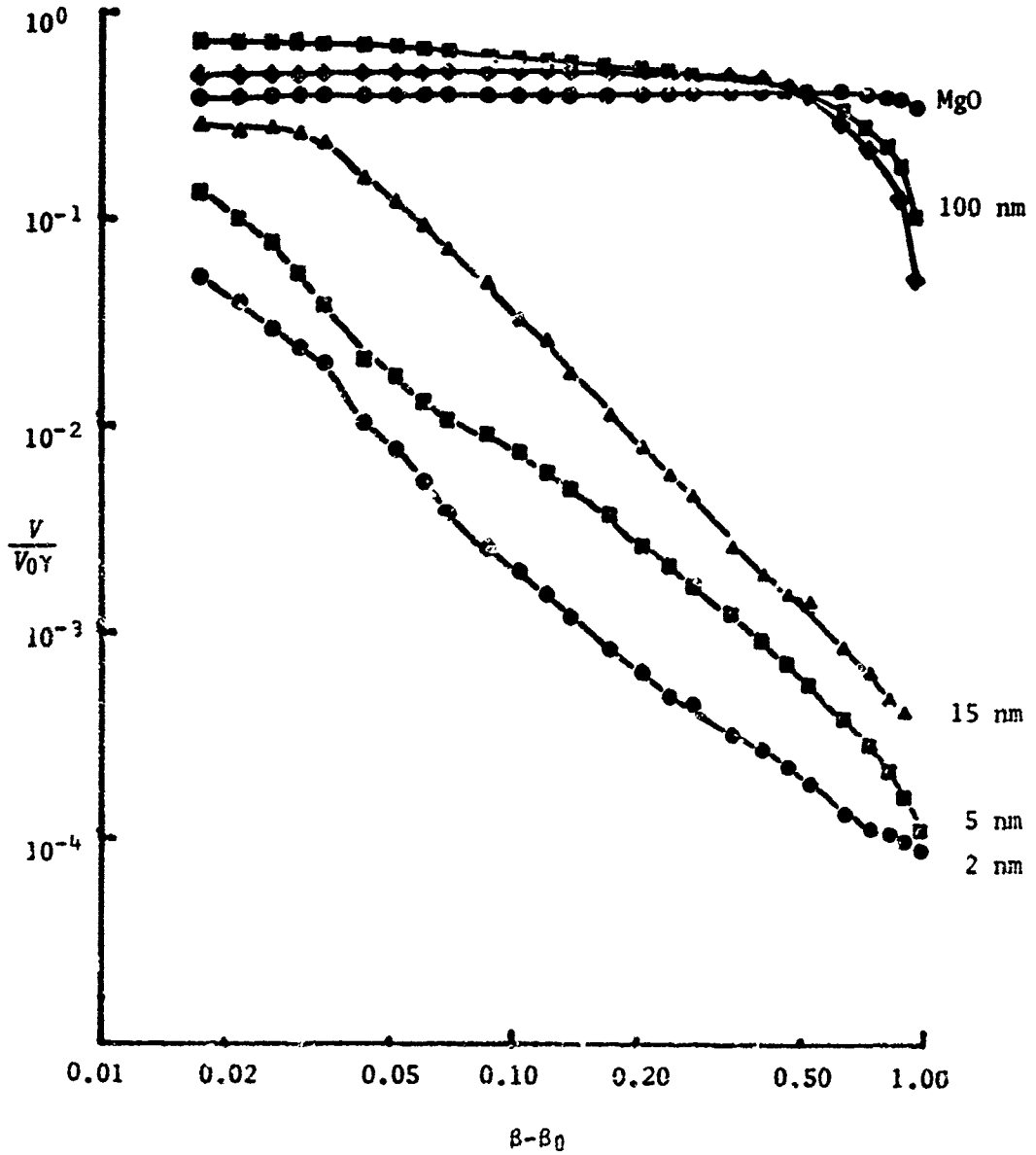

Fig. 25. Comparison of Scatter Prifiles for Samples with a Wide Range of Surface Roughnesses for a Normally Incident Beam.

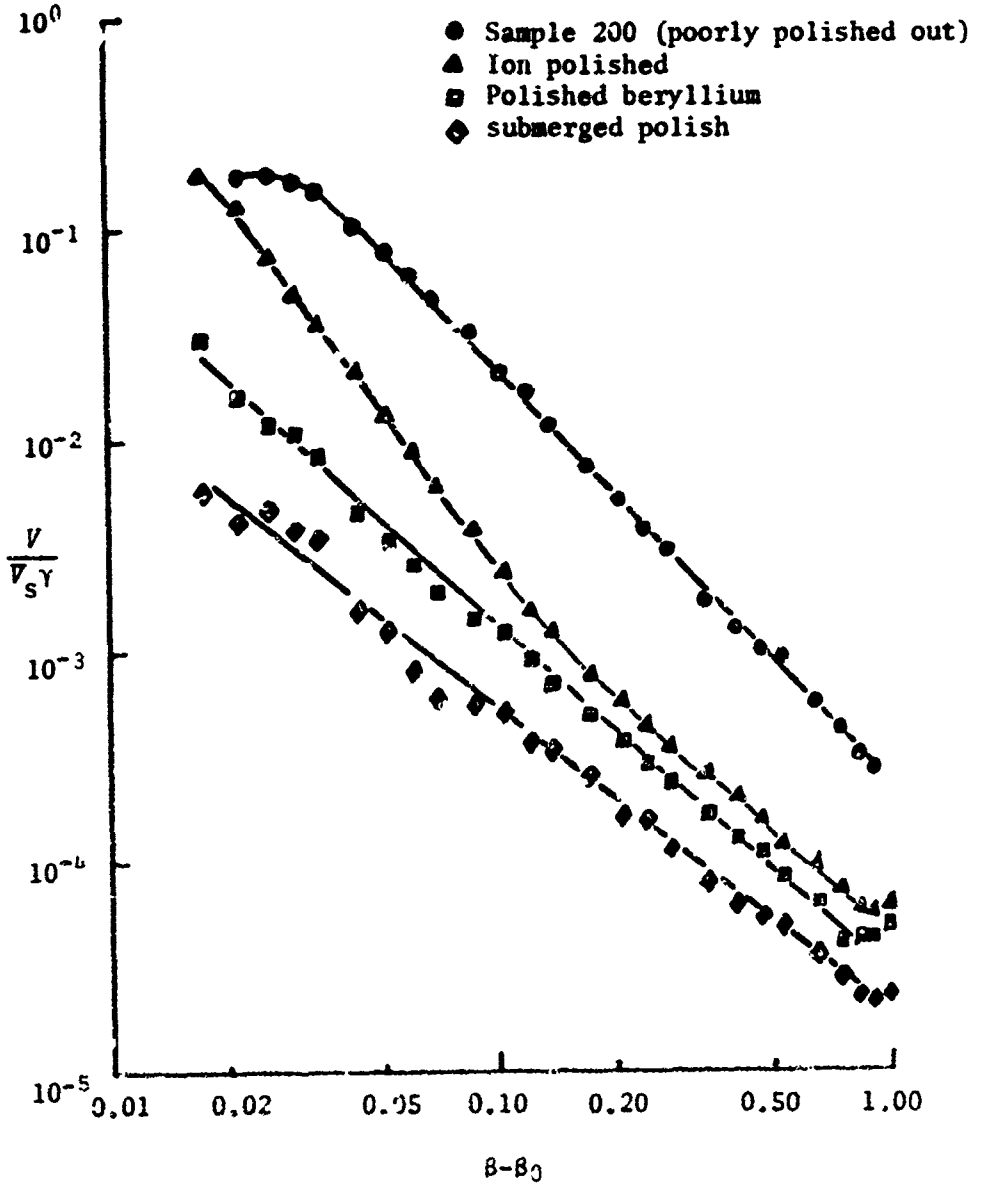

Fig. 26. Comparison of Scatter Profiles from Special Materials and Unusual Fabrication Techniques with Those of Conventional Optical Surfaces.

CHAPTER V

SURFACE STRUCTURE MEASUREMENTS

Three traditional techniques for obtaining surface structure information involve profilometry, electron-microscopy, and FECO interferometry. Most profilometers provide too coarse a measurement for optical surfaces. The electron microscope works nicely on the rough ground glass surfaces but fails to yield sufficient information about the smooth polished surfaces. However, since it requires multiple reflections, the FECO interferometer works well on smooth surfaces with a strong specular beam but does not yield good results for the rough diffuse surfaces. The latter two complementary techniques will thus be utilized in our research effort.

Electron Microscopy

Surface profiles of the rough samples are determined from electron-micrograph stereo pairs using conventional stereo-photogrammetric techniques [Moffitt (1959)]. Nankivell (1963) discusses some of the stereo-photogrammetric problems unique to electron microscope applications. A typical electron-micrograph stereo pair is shown in Fig. 27a with a line scribed to indicate the position of a set of preliminary surface height measurements that were made with a standard Fairchild Stereocomparagraph. This instrument consists of a mirror

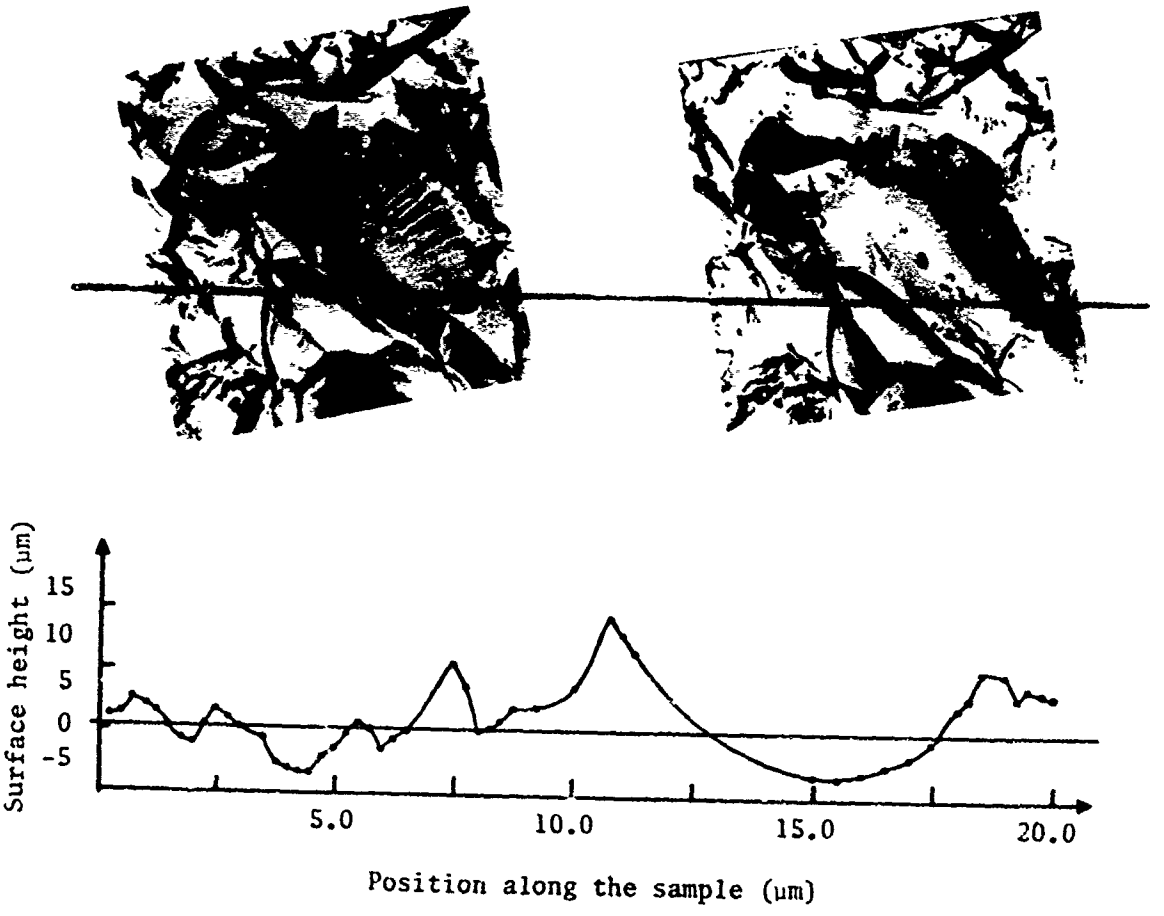

Fig. 27. (a) Typical Electron-Micrograph Stereo Pair of a Ground Glass Surface. (b) Surface Profile of Ground Glass Sample as Determined by Stero-Photogrammetric Techniques.

stereoscope fitted with a parallax bar containing a micrometer for measuring the parallax of each desired pair of points. The resulting surface profile is shown in Fig. 27b.

The two statistical parameters which determine the scattered light characteristics are the variance of the surface height distribution and the surface autocovariance function. A computer program was written which takes the surface profile data and determines the above two parameters. The transfer function of the scattering surface is then calculated from Eq. (48) of Chapter III. The Fourier transform of this function then yields the predicted scattered light distribution.

A Hewlett-Packard Model 9810 programmable desktop calculator and plotter is used for this data reduction. The program has only recently been debugged and become operational.

Figure 28 shows several sections of a surface profile, a histogram indicating the surface height distribution along with a gaussian function for comparison, the surface autocovariance function, the resulting transfer function, and finally the scattering function or spread function.

As this is a very recent result and due to some scaling problems in the computer program, a comparison of this predicted spread function with the measured scattering function is not yet available. This work is being continued under Contract F04701-75-C-0106.

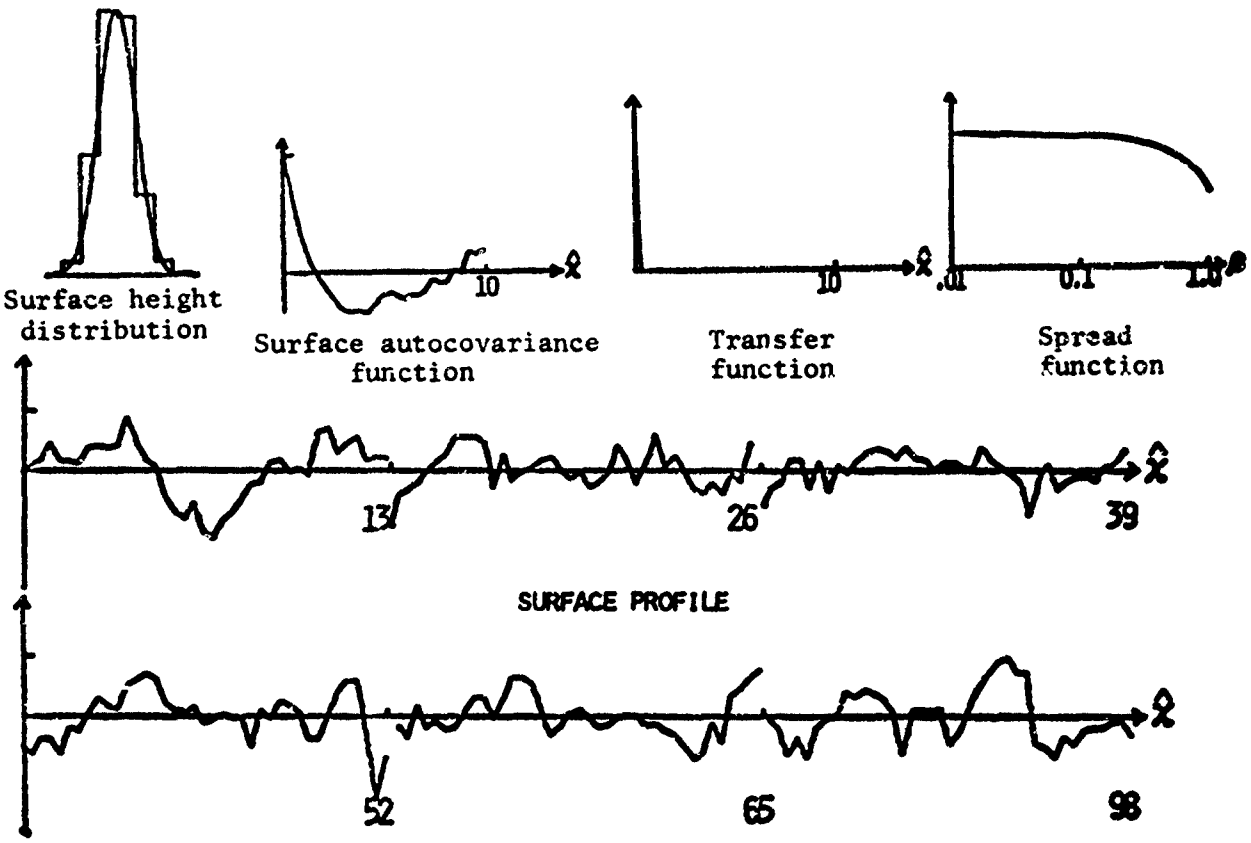

Fig. 28. Surface Profile of Ground Glass Sample and Its Associated Surface Height Distribution and Autocovariance Function.

The resulting transfer function and predicted spread function are also shown.

FECO Interferometry

Surface profiles of the smooth samples will be made with a FECO interferometer. This data will also be used to determine the variance of the surface height distribution and the surface autocovariance function. Bennett (1974) has reported on a scanning FECO interferometer that can measure very small height differences with a lateral resolution of 2 microns to yield statistics for optical surfaces. This instrument, along with auxiliary equipment which includes a slow-scan TV camera, signal averager, mini-computer, and a teletype unit, yields the surface profile, rms roughness, surface height distribution function, autocovariance function, and other statistical parameters for the surface.

We have sent two samples to be measured with the above apparatus. Additional samples will be measured on a Hilger Watts N130 FECO interferometer here at the Optical Sciences Center. The results of these measurements will be used to predict a surface spread function by applying the theory of Chapter III. This predicted spread function will then be compared to the directly measured scattering function in an attempt to experimentally verify our scattering theory. The results of this work will be reported under Contract F04701-75-C-0106.

CHAPTER VI

SUMMARY

A theoretical model to explain surface scatter has been developed in which the scattering process is assumed to be a diffraction phenomena.

By describing the diffraction process in terms of the direction cosines of the propagating light we have obtained the extremely powerful result that the diffracted wave field on an observation hemisphere is given directly by the Fourier transform of the aperture function. This allows us to apply the well-known techniques of linear systems theory that have proven so useful in the area of image formation. Furthermore, we have shown that any departures of the actual diffracted wave field from that predicted by the Fourier transform relationship take the form of conventional aberrations whose behavior is well understood in terms of the dimensions of the diffraction aperture, the radius of the observation hemisphere, and the appropriate field parameters.

This diffraction theory is then generalized to include the scattering effects of rough surfaces. For certain surfaces with well-behaved statistics, our theory predicts that, if the data collected on a hemisphere is plotted as a function of the direction cosines of the observation point, this new scattering function, which depends only upon the variance of the surface height distribution and the surface

autocovariance function, will not change shape but will merely be shifted in direction cosine space with changes in angle of incidence. This is a rather significant development, which has profound implications regarding the quantity of data required to completely characterize a scattering surface. No approximations are made in the theoretical development concerning the size of the surface height variations; hence, this theory should work equally well for very smooth, highly-polished optical surfaces and the very rough surfaces frequently used for baffle materials.

An instrument has been designed and built at the Optical Sciences Center for making scattered light measurements (or BRDF measurements) in an attempt to verify the above theory. This instrument is capable of making measurements over the entire hemisphere bounded by the plane of the sample (with an angular resolution of less than one degree) for any desired angle of incidence.

Extensive scatter measurements at a variety of angles of incidence have been made on two representative surfaces. One is a ground glass surface that is a very diffuse reflector. The other is an optically-polished surface that is a nice specular reflector. Both samples were aluminized prior to making the measurements. This data was then plotted as a function of the direction cosines of the position vector of the observation point. For the case of the smooth sample, the five curves with the angle of incidence varying from zero to 60 degrees coincide almost perfectly. The scattering curves for the rough sample

coincide for a substantial range of angles then begin to depart somewhat at large angles. The data from these two surfaces confirm that for a certain class of surfaces (in which optically-polished glass is definitely a member, and ground glass can perhaps be included to a lesser degree) the scattering properties of the surface are indeed shift invariant, and can be completely characterized by a single set of measurements at a fixed angle of incidence.

Surface profile measurements have been made on the rough sample from electron-micrograph stereo pairs using conventional stereo-photogrammetric techniques. Similar data will be obtained from a FECO interferometer for the smooth sample. A computer program has been written that takes the surface profile data and determines the variance of the surface height distribution and the surface autocovariance function. These two statistical parameters are then used to calculate the effective transfer function of the scattering surface. The Fourier transform of this quantity yields the predicted spread function or scattering function, which can then be directly compared to the measured scattered light distribution. This work is being continued under Contract F04701-75-C-0106.

The above developments indicate that the inverse scattering problem (determining surface properties from scattered light measurements) may become far more attractive than measuring surface properties directly.

APPENDIX A

FRESNEL AND FRAUNHOFER DIFFRACTION

In order to simplify the calculation of diffracted wave fields, it is customary to impose the restriction that the observation distance z in Eq. (15) be much larger than the maximum linear dimension of the diffracting aperture or the region of interest on the observation plane. Under this condition the term with $(1 + \delta)^2$ in the denominator will not differ significantly from unity and the quantity $(\hat{\ell} - \hat{z})$ in the exponent is adequately approximated by retaining only the first two terms of the binomial expansion for $\hat{\ell}$,

$$\hat{\ell} - \hat{z} \approx \frac{(\hat{x}^2+\hat{y}^2) + (\hat{x}'^2+\hat{y}'^2) - 2(\hat{x}\hat{x}'+\hat{y}\hat{y}')}{2\hat{z}} . \tag{A.1}$$

A sufficient condition for the validity of the above expression is the following Fresnel approximation

$$\hat{z}^3 >> \frac{\pi}{4} [(\hat{x}-\hat{x}')^2 + (\hat{y}-\hat{y}')^2]^2_{max} . \tag{A.2}$$

Substituting Eq. (A.1) into Eq. (15) results in the familiar Fresnel diffraction integral

$$U(\hat{x},\hat{y};\hat{z}) = \frac{e^{i2\pi\hat{z}}}{i\hat{z}} e^{\frac{i\pi}{\hat{z}}(\hat{x}^2+\hat{y}^2)} \iint_{-\infty}^{\infty} U_o(\hat{x}',\hat{y}';0)\ e^{\frac{i\pi}{\hat{z}}(\hat{x}'^2+\hat{y}'^2)}$$

$$\times\ e^{-\frac{i2\pi}{\hat{z}}(\hat{x}\hat{x}'+\hat{y}\hat{y}')}\, d\hat{x}'d\hat{y}', \qquad (A.3)$$

which is valid in the Fresnel region defined by Eq. (A.2).

If the following more-stringent condition, called the Fraunhofer approximation, is imposed upon the observation distance,

$$\hat{z} \gg \pi(\hat{x}'^2 + \hat{y}'^2)_{max}\ , \qquad (A.4)$$

then the quadratic phase function in the above equation is approximately unity over the entire aperture. The diffracted wave field on an observation plane in the Fraunhofer region defined by Eq. (A.4) is thus given directly from the Fourier transform of the pupil function $U_o(\hat{x}',\hat{y}'0)$. This is the well-known Fraunhofer diffraction integral

$$U(\hat{x},\hat{y};\hat{z}) = \frac{e^{i2\pi\hat{z}}}{i\hat{z}} e^{\frac{i\pi}{\hat{z}}(\hat{x}^2+\hat{y}^2)} \iint_{-\infty}^{\infty} U_o(\hat{x}',\hat{y}';0)$$

$$\times\ e^{-\frac{i2\pi}{\hat{z}}(\hat{x}\hat{x}' + \hat{y}\hat{y}')}\, d\hat{x}'d\hat{y}'. \qquad (A.5)$$

However, the pupil function $U_o(\hat{x}',\hat{y}';0)$ is equal to the product of the complex amplitude transmittance of the diffracting aperture (aperture function) $T_o(\hat{x}',\hat{y}';0)$, and the complex amplitude distribution incident upon the aperture. Hence, only when a plane wave is incident

upon the aperture is the Fraunhofer diffraction pattern given directly by the Fourier transform of the aperture function

$$U(\hat{x},\hat{y};\hat{z}) = \frac{e^{i2\pi\hat{z}}}{i\hat{z}} e^{\frac{i\pi}{\hat{z}}(\hat{x}^2+\hat{y}^2)} \iint_{-\infty}^{\infty} T_o(\hat{x}',\hat{y}';0) \times e^{-\frac{i2\pi}{\hat{z}}(\hat{x}\hat{x}'+\hat{y}\hat{y}')} d\hat{x}'d\hat{y}'. \quad (A.6)$$

Note that an identical expression is obtained from the Fresnel diffraction formula if a spherical wave converging to the observation plane is incident upon the diffracting aperture

$$U_o(\hat{x}',\hat{y}';0) = T_o(\hat{x}',\hat{y}';0)\, e^{-\frac{i\pi}{\hat{z}}(\hat{x}'^2+\hat{y}'^2)}. \quad (A.7)$$

In both of the above cases the Fourier transform must be evaluated at $\alpha = \hat{x}/\hat{z}$ and $\beta = \hat{x}/\hat{z}$ to assure proper space scaling in the observation plane.

APPENDIX B

CALCULATION OF ABERRATION COEFFICIENTS FOR DIFFRACTED WAVE FIELDS

For the case of a plane wave incident upon an aperture, the diffracted wave field on an observation plane is given by Eqs. (16) and (17), where

$$\hat{W} = (\hat{\ell}-\hat{z}) + (\hat{x}'\hat{x} + \hat{y}'\hat{y})/\hat{z}. \tag{B.1}$$

The quantity $\hat{\ell}$ can be written as

$$\hat{\ell} = \sqrt{(\hat{x}-\hat{x}')^2 + (\hat{y}-\hat{y}')^2 + \hat{z}^2}$$

$$= \hat{z}\sqrt{1 + [\hat{s}^2+\hat{s}'^2 - 2(\hat{x}\hat{x}'+\hat{y}\hat{y}')]/\hat{z}^2}, \tag{B.2}$$

where

$$\hat{s}^2 = \hat{x}^2 + \hat{y}^2, \qquad \hat{s}'^2 = \hat{x}'^2 + \hat{y}'^2.$$

A binomial expansion of the above square root results in the following expression for $\hat{W}$

$$\hat{W} = \frac{\hat{z}}{2}[\hat{s}^2 + s'^2]/\hat{z}^2$$

$$- \frac{\hat{z}}{8}[\hat{s}^4 + \hat{s}'^4 + 4(\hat{x}\hat{x}'+\hat{y}\hat{y}')^2 + 2\hat{s}^2\hat{s}'^2 - 4\hat{s}^2(\hat{x}\hat{x}'+\hat{y}\hat{y}')$$

$$- 4s'^2(xx'+yy')]/z^4$$

$$+ \text{higher-order terms.} \tag{B.3}$$

If we assume a rotationally-symmetric diffracting aperture we can, without loss of generality, choose the observation point on the $\hat{y}$-axis. Let us therefore set $\hat{x} = 0$. We can then let $\hat{s} = \hat{y}$ and $\hat{y}' = \hat{s}' \cos\phi$, hence

$$\hat{W} = \frac{\hat{z}}{2}\,[\hat{y}^2 + \hat{s}'^2]/\hat{z}^2$$

$$- \frac{\hat{z}}{8}\,[\hat{y}^4 + \hat{s}'^4 + 4\hat{y}^2\hat{s}'^2\cos^2\phi + 2\hat{y}^2\hat{s}'^2 - 4\hat{y}^3\hat{s}'\cos\phi - 4\hat{y}\hat{s}'^3\cos\phi]/\hat{z}^4$$

$$+ \text{higher-order terms.} \qquad \text{(B.4)}$$

If we now substitute

$$\hat{y} = \rho\hat{y}_{max}, \qquad \hat{s}' = \hat{a}\,\frac{\hat{d}}{2}$$

into the previous equation, we obtain

$$\hat{W} = \frac{\hat{z}}{2}\,[\hat{y}_{max}^2\,\rho^2 + (\hat{d}/2)^2\,\hat{a}^2]/\hat{z}^2$$

$$- \frac{\hat{z}}{8}\,[\hat{y}_{max}^4\,\rho^4 + (\hat{d}/2)^4\,\hat{a}^4 + 4\hat{y}_{max}^2\,(\hat{d}/2)^2\,\rho^2\hat{a}^2\cos^2\phi + 2\hat{y}_{max}^2\,(\hat{d}/2)^2\,\rho^2\hat{a}^2 - 4\hat{y}_{max}^3\,(\hat{d}/2)\,\rho^3\hat{a}\cos\phi - 4\hat{y}_{max}^3\,(\hat{d}/2)^3\,\rho\hat{a}^3\cos\phi]/\hat{z}^4$$

$$+ \text{higher-order terms.} \qquad \text{(B.5)}$$

Equating coefficients of corresponding terms between this equation and the wavefront aberration function given by Eq. (24), we obtain the aberration coefficients tabulated in the first column of Table 1.

If we now have a spherical wave incident upon the aperture, the quantity $\hat{W}$ in Eq. (17) is given by

$$\hat{W} = (\hat{\ell}-\hat{z}) - (\hat{\ell}_o-\hat{z}) + (\hat{x}\hat{x}' + \hat{y}\hat{y}')/\hat{z}, \tag{B.6}$$

where

$$\hat{\ell}_o = \sqrt{\hat{x}'^2 + \hat{y}'^2 + \hat{z}^2} = \hat{z}\sqrt{1 + \hat{s}'^2/\hat{z}^2}.$$

A binomial expansion of this quantity results in

$$\hat{\ell}_o - \hat{z} = \frac{\hat{z}}{2}(\hat{s}'/\hat{z})^2 - \frac{\hat{z}}{8}(\hat{s}'/\hat{z})^4 + \ldots \tag{B.7}$$

But these will merely cancel identical terms in the previous expansion thus resulting in the aberration coefficients presented in column two of Table 1.

For the case of a hemispherical observation space the diffracted wave field is given by Eqs. (22) and (23). With a plane wave incident upon the aperture, we have

$$\hat{W} = (\hat{\ell}-\hat{r}) + (\alpha\hat{x}' + \beta\hat{y}'). \tag{B.8}$$

The quantity $\hat{\ell}$ can be written as

$$\ell = \sqrt{(\hat{x}-\hat{x}')^2 + (\hat{y}-\hat{y}')^2 + \hat{z}^2}$$

$$= \hat{r}\sqrt{1 + [\hat{s}'^2 - 2\hat{r}(\alpha\hat{x}' + \beta\hat{y}')]/\hat{r}^2}, \tag{B.9}$$

where

$$\hat{s}'^2 = \hat{x}'^2 + \hat{y}'^2, \qquad \hat{r}^2 = \hat{x}^2 + \hat{y}^2 + \hat{z}^2.$$

A binomial expansion of the above square root yields

$$\hat{W} = \frac{\hat{r}}{2}(\hat{s}'/\hat{r})^2 - \frac{\hat{r}}{8}[\hat{s}'^4 - 4\hat{r}\hat{s}'^2(\alpha\hat{x}'+\beta\hat{y}') + 4\hat{r}^2(\alpha\hat{x}'+\beta\hat{y}')^2]/\hat{r}^4$$

$$+ \text{higher-order terms.} \qquad \text{(B.10)}$$

If we again assume a rotationally-symmetric diffracting aperture we can, without loss of generality, choose the observation point on the $\hat{y}$-axis. Let us therefore set $\alpha = 0$. We can also let $\hat{y}' = \hat{s}' \cos\phi$ which results in

$$\hat{W} = \frac{\hat{r}}{2}(\hat{s}'/\hat{r})^2 - \frac{\hat{r}}{8}[\hat{s}'^4 - 4\hat{r}\beta\hat{s}'^3\cos\phi + 4\hat{r}^2\beta^2\hat{s}'^2\cos^2\phi]/\hat{r}^4$$

$$+ \text{higher-order terms.} \qquad \text{(B.11)}$$

If we now substitute

$$\beta = \rho\beta_{max}, \qquad \hat{s}' = \hat{a}\frac{\hat{d}}{2}$$

into the previous equation, we obtain

$$\hat{W} = \frac{\hat{r}}{2}(\hat{d}/2\hat{r})^2\hat{a}^2 - \frac{\hat{r}}{8}[(\hat{d}/2)^4\hat{a}^4 - 4\hat{r}\beta_{max}(\hat{d}/2)^3\beta\rho^3\cos\phi$$

$$+ 4\hat{r}^2\beta_{max}^2(\hat{d}/2)^2\beta^2\rho^2\cos^2\phi]/\hat{r}^4$$

$$+ \text{higher-order terms.} \qquad \text{(B.12)}$$

Again equating coefficients of corresponding terms between this equation and the wavefront aberration function given by Eq. (24), we obtain the aberration coefficients tabulated in column three of Table 1.

If we now have a spherical wave illuminating the aperture and a hemispherical observation space, the quantity $\hat{W}$ in Eq. (23) is given by

$$\hat{W} = (\hat{\ell}-\hat{r}) - (\hat{\ell}_o-\hat{r}) + (\alpha\hat{x}' + \beta\hat{y}'), \tag{B.13}$$

where

$$\hat{\ell}_o = \sqrt{\hat{x}'^2 + \hat{y}'^2 + \hat{r}^2} = \hat{r}\sqrt{1 + \hat{s}'^2/\hat{r}^2}.$$

A binomial expansion of this quantity results in

$$\hat{\ell}_o - \hat{r} = \frac{\hat{r}}{2}(\hat{s}'/\hat{r})^2 - \frac{\hat{r}}{8}(\hat{s}'/\hat{r})^4 + \ldots \quad . \tag{B.14}$$

Once again these terms merely cancel identical terms in the previous expansion, leaving only coma and astigmatism present in the diffracted wave field as indicated in the last column of Table 1.

APPENDIX C

BIDIRECTIONAL REFLECTANCE DISTRIBUTION FUNCTION

The basic quantity that characterizes (geometrically) the reflecting properties of a surface element dA is the bidirectional reflectance distribution function (BRDF). This quantity

$$f_r(\theta_i,\phi_i;\ \theta_r,\phi_r) = dL_r(\theta_i,\phi_i;\ \theta_r,\phi_r;\ E_i)/dE_i(\theta_i,\phi_i)$$

$$= dL_r(\theta_i,\phi_i;\ \theta_r,\phi_r;\ E_i)/L_i(\theta_i,\phi_i)d\Omega_i \quad (sr^{-1}) \tag{C-1}$$

is defined by Nicodemus (1970), as the reflected radiance $dL_r(\theta_i,\phi_i;\ \theta_r,\phi_r;\ E_i)$ of the surface element dA in the direction (θ_r,ϕ_r) divided by the incident irradiance $dE_i(\theta_i,\phi_i) = Li(\theta i,\phi i)d\Omega i$ producing it. The geometry of this situation is illustrated in Fig. 29, where the element of projected solid angle is given by $d\Omega \equiv \cos\theta d\omega$.

The numerical value of the BRDF for a given pair of incident and reflected ray directions may vary from zero to infinity. In particular, consider two ideal cases. The BRDF is a constant for all reflected directions for a perfectly diffuse (Lambertian) surface; and it becomes infinite (as a Dirac delta function) for a perfectly specular reflector. The BRDF, defined above as a ratio of infinitesimals, is an idealized concept that can never be measured exactly. Real measurements are

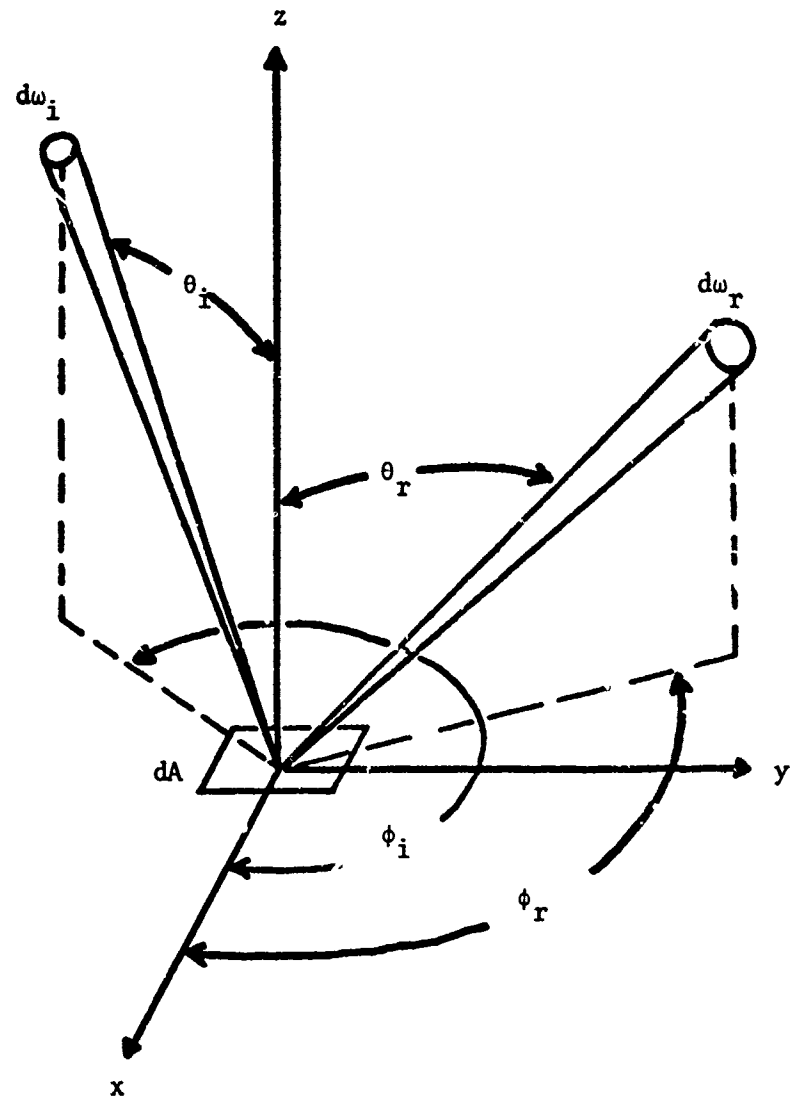

Fig. 29. Geometry of Incident and Reflected Elementary Beams Used to Define the Bidirectional Reflectance Distribution Function.

always made over some finite solid angle and wavelength interval and can therefore yield only average values $\overline{f_r}$ over those parameter intervals.

The BRDF is basic in the sense that all other reflectance or scattering functions can be derived from it. For example, Judd (1967) lists nine different kinds of reflectance functions based on the angular extent of the incident and reflected radiation. All of them can be derived from the BRDF.

Note that the BRDF is a four-dimensional quantity that can be thought of as an infinite family of two-dimensional light distribution functions--one for every possible angle at which the incident beam can strike the surface element. This involves an overwhelming quantity of data, especially where high directional resolution is needed to describe glints and specularities.

APPENDIX D

LITERATURE REVIEW

The following listing serves as a bibliography for this report as well as an update of the literature review initiated under Contract F04701-72-C-0181.

Ament, W. S., 1953, "Toward a Theory of Reflection by a Rough Surface," Proc. IRE 41:142.

_____, 1956, "Forward- and Back-Scatter from Certain Rough Surfaces," IRE Trans. AP-4:369-373.

_____, 1960, "Reciprocity and Scattering by Certain Rough Surfaces," IRE Trans. AP-8:167-174.

Asubakar, I., 1962, "Scattering of Plane Elastic Waves at Rough Surfaces. I.," Proc. Cambridge Phil. Soc. 58:136-57.

Bachynski, M. P., 1959, "Microwave Propagation over Rough Surfaces," RCA Review 20:308-335.

Barrick, D. E., 1965, "Two Experiments Yielding Lunar Surface Information Employing Polarized Radar Waves," Ohio State University Research Foundation, Columbus, Ohio. (Available from the National Technical Information Service, No. N66-14962.)

_____, 1965, "A More Exact Theory of Backscattering from Statistically Rough Surfaces," Ohio State University Research Foundation, Columbus, Ohio, Report 1388-18. (Available from the National Technical Information Service, No. N66-14963.)

_____, 1965, "Determination of RMS Height of a Rough Surface Using Radar Waves," Ohio State University Research Foundation, Columbus, Ohio, Report 1388-19. (Available from the National Technical Information Service, No. N66-14956.)

_____, 1965, "Theoretical Curves of Backscattering Cross Sections of Rough Surfaces for Several Polarization States Using Two Statistical Models," Ohio State University Research Foundation, Columbus, Ohio, Report 1388-20. (Available from the National Technical Information Service, No. N66-10957.)

_____, and W. H. Peake, 1967, "Scattering from Surfaces with Different Roughness Scales: Analysis and Interpretation," Battelle Memorial Institute, Columbus, Ohio, Report BAT-197A-10-3. (Available from Clearinghouse for Federal Scientific and Technical Information, Springfield, Virginia, No. AD 662751.)

_____, 1968, "Rough Surface Scattering Based on the Specular Point Theory," IEEE Trans. AP-16:449-454.

_____, 1970, "Rough Surfaces," *Radar Cross Section Handbook*, Vol. 2, G. T. Ruck, et al., eds., (Plenum Press, New York), pp. 671-772.

_____, 1970, "The Interaction of RF/VHF Radio Waves with the Sea Surface and its Implications," *AGARD Conference on Electromagnetics of the Sea* (Paris, France), pp. 18-1 to 18-25. (Available from Clearinghouse for Federal Scientific and Technical Information, Springfield, Virginia, No. AD 716350)

Bass, F. G., et al., 1968, "Very High Frequency Radiowave Scattering by a Disturbed Sea Surface," IEEE Trans. AP-16:554-568.

Beaglehole, D., 1970, "Optical Excitation of Surface Plasmons," IEEE Trans. ED-17:240-244.

_____, and O. Hunderi, 1970, "Study of the Interaction of Light with Rough Metal Surfaces," Phys. Rev. B 2:309-329.

Beard, C. I., 1961, "Coherent and Incoherent Scattering of Microwaves from the Ocean," IRE Trans. AP-9:470-483.

Beckmann, P., 1957, "A New Approach to the Problem of Reflection from a Rough Surface," Acta. Techn. CSAV. 2:311-355.

_____, 1961, "The Scattering of Waves by a Periodic Surface," Czech. J. Phys. 11:863-70.

Bennett, H. E., and J. O. Porteus, 1961, "Relation Between Surface Roughness and Specular Reflectance at Normal Incidence," J. Opt. Soc. Am. 51:123-9.

_____, 1963, "Specular Reflectance of Aluminized Ground Glass and the Height Distribution of Surface Irregularities," J. Opt. Soc. Am. 53:1389-94.

Bennett, J., 1974, "Use of Interferometry for Determining the rms Roughness, Autocovariance Function, and Other Statistical Properties of Optical Surfaces," (Abstract) J. Opt. Soc. Am. 64:1362.

Biot, M. A., 1957, "Some New Aspects of the Reflection of Electromagnetic Waves on a Rough Surface," J. Appl. Phys. 28:1455-1462.

Birkebak, R. C., 1962, "Monochromatic Directional Distribution of Reflected Thermal Radiation from Roughened Surfaces," Ph.D. Dissertation in Engineering, Mechanical Engineering Department, University of Minnesota, Minneapolis, Minnesota.

_____, et al., 1964, "Effect of Surface Roughness on the Total Hemispherical and Specular Reflectance of Metallic Surfaces," J. Heat Transfer, Trans. ASME 86:193-199.

Blake, L. V., 1950, "Reflection of Radio Waves from a Rough Sea," Proc. IRE 38:301-304.

Bloembergen, N., and Y. R. Shen, 1965, "Coupling of Light with Phonons, Magnons, and Plasmons," Phys. of Quantum Elect., Conference Proceedings, P. L. Kelley, et al., eds., San Juan, Puerto Rico (McGraw-Hill, New York), pp. 119-128.

Bojarski, N. N., 1971, "Electromagnetic Inverse Scattering," Mathematics of Profile Inversion Workshop, Ames Research Center, Moffett Field, California, L. Colin, ed., pp. 6-34 to 6-37 (NASA TM X-62, 150). (Available from the National Technical Information Service, No. N73-11615.)

Booker, H. G., J. A. Ratcliffe, and D. H. Shinn, 1950, "Diffraction from an Irregular Screen with Applications to Ionospheric Problems," Phil. Trans. Roy. Soc. London 242:579-607.

Born, M., and E. Wolf, 1965, *Principles of Optics*, ed. 3 (Pergamon Press, New York).

Bracewell, R. N., 1965, *The Fourier Transform and its Applications* (McGraw-Hill, New York).

Briggs, B. H., 1961, "Diffraction by an Irregular Screen of Limited Extent," Proc. Phys. Soc. 77:305-17.

Brockelmen, R. A., and T. Hagfors, 1966, "Note on the Effect of Shadowing on the Backscattering of Waves from a Random Rough Surface," IEEE Trans. AP-14:621-629.

Burrows, M. L., 1969, "Equivalence of the Rayleigh Solution and the Extended-Boundary-Condition Solution for Scattering Problems," Elect. Lett. 5:277-278.

Carmer, W. C., and M. E. Bair, 1969, "Some Polarization Characteristics of Magnesium Oxide and other Diffuse Reflectors," Appl. Opt. 8:1597.

Chenmoganadam, T. K., 1919, "On the Specular Reflection from Rough Surfaces," Phys. Rev. 13:96-101.

Church, E. L., and J. M. Zavada, 1975, "Residual Surface Roughness of Diamond-Turned Optics," Appl. Opt. 14:1788.

Clark, R. H., and G. O. Hendry, 1964, "Prediction and Measurement of the Coherent and Incoherent Power Reflected from a Rough Surface," IEEE Trans. AP-12:353-363.

Crane, R. B., 1970, "Use of a Laser-Produced Speckle Pattern to Determine Surface Roughness," J. Opt. Soc. Am. 60:1658-1663.

Crowell, J., and R. H. Ritchie, 1970, "Surface Plasmon Effect in the Reflectance of a Metal," J. Opt. Soc. Am. 60:794-799.

Eckart, C., 1953, "The Scattering of Sound from the Sea Surface," J. Acoust. Soc. Am. 25:566-570.

Daniels, F. B., 1961, "A Theory of Radar Reflection from the Moon and Planets," J. Geophys. Res. 66:1781-1788.

_____, 1963, "Radar Determination of the Root Mean Square Slope of the Lunar Surface," J. Geophys. Res. 68:449-453.

Daudé, A., A. Savary, and S. Robin, 1972, "Effects of Different Roughnesses on the Excitation by Photons of the Surface Plasmon of Aluminum," J. Opt. Soc. Am. 62:1-5.

Davies, H., 1954, "The Reflection of Electromagnetic Waves from a Rough Surface," Proc. IEEE 101:209-14.

DeBell, M. A., and J. E. Harvey, 1974, "Recent Developments in Surface Scatter Studies," (Abstract) J. Opt. Soc. Am. 64:1404.

Devaney, A. J., and G. C. Sherman, 1973, "Plane-Wave Representations for Scalar Wave Fields," SIAM Review 15:765.

Eastman, J. M., and P. W. Baumeister, 1974, "Measurement of the Microtopography of Optical Surfaces using a Scanning Fizeau Interferometer," (Abstract) J. Opt. Soc. Am. 64:1369.

Elson, J. M., and R. H. Ritchie, 1971, "Photon Interactions at a Rough Metal Surface," Phys. Rev. B 4:4129-4138.

Evans, J. V., and G. H. Pettengill, 1963, "The Scattering Behavior of the Moon at Wavelengths of 3.6, 68, and 784 Centimeters," J. Geophys. Res. 68:423-447.

Feinstein, J., 1954, "Some Stochastic Problems in Wave Propagation," Part I. Trans. IRE AP-2:23-30.

Fuks, I. M., 1966, "Theory of Radio Wave Scattering at a Rough Sea Surface," Soviet Radiophysics 9:513-519.

Fung, A. K., and R. K. Moore, 1964, "Effects of Structure Size on Moon and Earth Radar Returns at Various Angles," J. Geophys. Res. 69:1075-1081.

_____, 1964, "Theory of Radar Scatter from Rough Surfaces, Bistatic and Monostatic, with Applications to Lunar Radar Return," J. Geophys. Res. 69:1063-1073.

_____, 1965, "Scattering and Depolarization of Electromagnetic Waves by Rough Surfaces," Center for Research on Engineering Science, University of Kansas, Lawrence, Kansas, CRES Report 48-5. (Available from the National Technical Information Service, No. N68-100004.)

_____, 1966, "Scattering and Depolarization of EM Waves from a Rough Surface," Proc. IEEE 54:395-396.

_____, and R. K. Moore, 1966, "The Correlation Function in Kirchhoff's Method of Solution of Scattering of Waves from Statistically Rough Surfaces," J. Geophys. Res. 71:2939-2943.

_____, 1966, "On Depolarization of Electromagnetic Waves Backscattered from a Rough Surface," Planetary and Space Science, 14:563-568.

_____, 1967, "Theory of Cross Polarized Power Returned from a Random Surface," Appl. Sci. Res. 18:50-60.

_____, 1967, "Character of Wave Depolarization by a Perfectly Conducting Rough Surface and Its Application to Earth and Moon Experiments," Planetary and Space Science 15:1337-1347.

_____, 1968, "Mechanisms of Polarized and Depolarized Scattering from a Rough Dielectric Surface," Franklin Institute J. 285:125-133.

_____, 1969, "Backscattering of Waves by Composite Rough Surfaces," IEEE Trans. AP-17:590-597.

_____, 1970, "Scattering and Depolarization of Electromagnetic Waves from a Slightly Rough Dielectric Layer," Canadian J. Phys. 48:127-136.

_____, and H. L. Chan, 1970, "Depolarization of EM Waves by Rough Surfaces," IEEE International Symposium on Electromagnetic Compatibility, Anaheim, California, pp. 228-231.

_____, and H. L. Chan, 1971, "On the Integral for Backscattering from a Randomly Rough Surface," Proc. IEEE 59:1280-1281.

Garrod, R. I., and J. F. Nankivell, 1958, "Sources of Error in Electron Stereomicrocopy," Brit. J. Appl. Phys. 9:214.

Goodman, J. W., 1968, *Introduction to Fourier Optics* (McGraw-Hill, San Francisco).

Hagfors, T., 1964, "Backscattering from an Undulating Surface with Applications to Radar Returns from the Moon," J. Geophys. Res. 69:3779-3784.

Heinisch, R. P., 1971, "Infrared Mirror-Scatter Measurements," J. Opt. Soc. Am. 61:1225-1229.

Hodgkinson, I. J., 1970, "The Application of Fringes of Equal Chromatic Order to the Assessment of the Surface Roughness of Polished Fused Silica," J. Phys. E. Sci. Instr. 3:300-304.

_____, 1970, "A Simple Scatter Method for Optical Surface Roughness and Slope Measurements. Roughness of Polished Fused Silica," J. Phys. E. Sci. Instr. 3:341.

Hopkins, H. H., 1950, *Wave Theory of Aberrations* (Oxford Clarendon Press, London).

Hudson, R. D., 1969, *Infrared System Engineering* (John Wiley & Sons, New York).

Hunderi, O., and D. Beaglehole, 1970, "Study of the Interaction of Light with Rough Metal Surfaces. II. Theory," Phys. Rev. B 2:321-329.

Ingelstam, E., and P. J. Lindberg. 1954, "Optical Image Evaluation," National Bureau of Standards Circular 526, Chap. 12.

Isakovich, M. A., 1952, "The Scattering of Waves from a Statistically Rough Surface," Zhurn. Eksp. Theor. Fiz. 23:305-314. (Translation available from Defense Scientific Information Service, DRB Canada, T 112 R.)

Kiracek, G. R., 1973, "Numerical Comparisons of a Modified Rayleigh Approach with Other Rough Surface EM Scattering Solutions," IEEE Trans. AP-21:393-396.

Judd, D. B., 1967, "Terms, Definitions, and Symbols in Reflectometry," J. Opt. Soc. Am. 57:445-452.

Kapany, K. S., J. J. Burke, Jr., and K. Frame, 1965, "Diffraction by Apertures of Wavelength Dimensions," Appl. Opt. 4:1229.

Keller, J. B., 1962, "Geometrical Theory of Diffraction," J. Opt. Soc. Am. 52:116.

Kalor, E., 1968, "Conditions for the Validity of the Angular Spectrum of Plane Waves," J. Opt. Soc. Am. 58:1235.

Leader, J. C., 1970, "Bidirectional Scattering of Electromagnetic Waves from Rough Surfaces," McDonnell Aircraft Company, St. Louis, Missouri, MDC 70-022.

_____, 1970, "Multiple Scattering of Electromagnetic Waves from Rough Surfaces," McDonnell Aircraft Company, St. Louis, Missouri, MDC 70-037.

_____, 1971, "Spectral and Angular Dependence of Specular Scattering from Rough Surfaces," McDonnell Aircraft Company, St. Louis, Missouri, MCAIR 71-013.

_____, 1971, "Bidirectional Scattering of Electromagnetic Waves from Rough Surfaces," J. Appl. Phys. 42:4808-4816.

_____, 1971, "The Relationship between the Kirchhoff Approach and Small Perturbation Analysis in Rough Surface Scattering Theory," IEEE Trans. AP-19:786-788.

_____, and W. A. J. Dalton, 1972, "Bidirectional Scattering of Electromagnetic Waves from the Volume of Dielectric Materials," J. Appl. Phys. 43:3080-3090.

_____, 1972, "Hemispherical Scattering of Electromagnetic Waves from Rough Surfaces," McDonnell Aircraft Company, St. Louis, Missouri, MCAIR 72-037.

Longuet-Higgins, M. S., 1959, "The Distribution of the Sizes of Images Reflected in a Random Surface," Proc. Cambridge Phil. Soc. 55:91-100.

McKenney, D. B., G. R. Orme, and L. P. Mott, 1972, "Light Scattering by Thin Film Coatings," Optical Sciences Center (Univ. of Ariz.) Final Report.

Mercier, R. P., 1961, "Diffraction by Finite Irregular Objects," Proc. Phys. Soc. 77:318-27.

_____, 1962, "Diffraction by a Screen Causing Large Random Phase Fluctuations," Proc. Cambridge Phil. Soc. 58:382-400.

Millar, R. F., 1969, "On the Rayleigh Assumption in Scattering by a Periodic Surface," Proc. Camb. Phil. Soc. 65:773-791.

_____, et al., 1969, "Rayleigh Hypothesis in Scattering Problems," Elect. Lett. 5:416-418.

_____, 1971, "On the Rayleigh Assumption in Scattering by a Periodic Surface. II.," Proc. Camb. Phil. Soc. 69:217-225.

Miller, E. R., and R. S. Vun Kannon, 1967, "Development and Use of a Bidirectional Spectroreflectometer," AIAA, Paper 67-313.

Moffitt, F. H., 1959, *Photogrammetry* (International Textbook Co.).

Mott, L. P., 1971, "The Effect of Surface Roughness on the Optical Properties of All-Dielectric Interference Filters," Master's Thesis (Univ. of Ariz.).

Motycka, J., 1969, "Proposed Interferometric Method of Measurement of Roughness and Autocorrelation Function in Smooth-Finished Surfaces," Appl. Opt. 8:1435-1438.

Murray, J. J., et al., 1971, "Proposed Supplement to the SI Nomenclature for Radiometry and Photometry," Appl. Opt. 10:1465-1468.

Nankivell, J. F., 1962, "Minimum Differences in Height Detectable in Electron Stereomicroscopy," Brit. J. Appl. Phys. 13:126.

_____, 1962, "Stereoscopic Viewing of Metal Foils in the Electron Microscope," Brit. J. Appl. Phys. 13:129.

_____, 1963, "The Theory of Electron Stereo Microscopy," Optic 20:171.

_____, 1965/1966, "Determination of Directed Distances in Objects Examined in the Electron Microscope," Optic 23:506.

Nicodemus, F. E., 1965, "Directional Reflectance and Emissivity of an Opaque Surface," Appl. Opt. 4:767.

_____, 1970, "Reflectance Nomenclature and Directional Reflectance and Emissivity," Appl. Opt. 9:1474-5.

Orme, G. R., 1972, "Measurement of Small Angle Scatter from Smooth Surfaces," Optical Sciences Center (Univ. of Ariz.) Tech. Rept. 74

Papoulis, A., 1965, *Probability, Random Variables, and Stochastic Processes* (McGraw-Hill).

Peake, W. H., 1959, "Interaction of Electromagnetic Waves with Some Natural Surfaces," Ph.D. Dissertation (Ohio State University).

_____, 1959, "Theory of Radar Return from Terrain," IRE National Convention Record 7:27-41.

_____, 1959, "Interaction of Electromagnetic Waves with Some Natural Surfaces," IRE Trans. AP-7.

Porteus, J. O., 1963, "Relation between the Height Distribution of a Rough Surface and the Reflectance at Normal Incidence," J. Opt. Soc. Am. 53:1394-1402.

Ratcliffe, J. A., 1956, "Some Aspects of Diffraction Theory and Their Application to the Ionosphere," in A. C. Strickland, ed., *Reports on Progress in Physics*, Vol. XIX (The Physical Society, London).

Rayleigh, Lord, 1901, "Polish," Nature 64:385-388.

_____, 1945, *The Theory of Sound*, Vol. II (Dover, New York).

Renau, J., and J. A. Collinson, 1965, "Measurements of Electromagnetic Backscattering from Known, Rough Surfaces," Bell System Tech. J. 44:2203-2227.

_____, et al., 1967, "Depolarization of Linearly Polarized EM Waves Backscattered from Rough Metals and Inhomogeneous Dielectrics," J. Opt. Soc. Am. 57:459-466.

Ribbins, W. B., 1969, "Interferometric Surface Roughness Measurement," Appl. Opt. 8:2173-2176.

_____, 1972, "Surface Roughness Measurement by Holographic Interferometry," Appl. Opt. 11:807-810.

Rice, S. O., 1965, "Reflections of Electromagnetic Waves by Slightly Rough Surfaces," *The Theory of Electromagnetic Waves*, M. Klein, ed., (Dover, New York).

Ritchie, R. H., et al., 1968, "Surface-Plasmon Resonance Effect in Grating Diffraction," Phys. Rev. Lett. 21:1530-1533.

Russell, D. A., 1960, "Spectral Reflectance of Rough Surfaces in the Infrared," Master's in Mechanical Engineering (Univ. of California. Berkeley).

Sancer, M. I., 1969, "Shadow-Corrected Electromagnetic Scattering from a Randomly Rough Surface," IEEE Trans. AP-17:577-585.

Scheele, S. R., 1973, "Scattering Characteristics of Mirrors and the Associated Inverse Scattering Problem," Ph.D. Dissertation (Univ. of California at Los Angeles).

_____, 1974, "Multispectral Measurements of BRDF for very Smooth Surfaces," AIAA Paper No. 74-671 (Thermophysics and Heat Transfer Conference, Boston, Massachusetts).

Shack, R. V., 1967, "Interaction of an Optical System with the Incoming Wavefront in the Presence of Atmospheric Turbulence," Optical Sciences Center (Univ. of Ariz.) Tech. Rept. 19.

_____, 1968, "Geometric vs. Diffraction Prediction of Properties of a Star Image in the Presence of an Isotropic Random Wavefront Disturbance," Optical Sciences Center (Univ. of Ariz.) Tech. Rept. 32.

_____, and M. A. DeBell, 1974, "Surface Scatter Study," Optical Sciences Center (Univ. of Ariz.) final report prepared for the Space and Missile Systems Organization under Contract F04701-72-C-0181.

Spetner, L. M., 1958, "A Statistical Model for Forward Scattering of Waves of a Rough Surface," Trans. IRE AP-6:88-94.

Stover, J. C., 1975, "Roughness Characterization of Smooth Machined Surfaces by Light Scattering," Appl. Opt. 14:1796.

Swift, C. T., 1971, "A Note on Scattering from a Slightly Rough Surface," IEEE Trans. AP-19:561-562.

Thompson, M. M., 1966, *Manual of Photogrammetry*, Vol. II (American Society of Photogrammetry).

Thompson, S. P., 1912, *Treatise on Light* (Macmillan & Co., London).

Twersky, V., 1950, "On the Non-Specular Reflection of Plane Waves of Sound, J. Acoust. Soc. Am. 22:539-546.

_____, 1951, "On the Nonspecular Reflection of Electromagnetic Waves," J. Appl. Phys. 22:825-835.

_____, 1957, "On Scattering and Reflection of Electromagnetic Waves by Rough Surfaces," IRE Trans., pp. 81-90.

_____, 1959, "Scattering by Quasi-Periodic and Quasi-Random Distributions," IRE Trans. AP-7:S307-S319.

_____, 1962, "On Scattering of Waves by Random Distributions. I. Free-Space Scatterer Formalism," J. Math. Phys. 3:700-715.

Vachaspati, 1964, "Scattering of Light by Free Electrons, Intensity Dependent Phase Shift and Frequency Change," Indian J. Pure and Appl. Phys. 2:373-376.

Valenzuela, G. R., 1967, "Depolarization of EM Waves by Slightly Rough Surfaces," IEEE Trans. AP-15:552-557.

_____, 1968, "Scattering of Electromagnetic Waves from a Tilted Slightly Rough Surface," Radio Sci. 3:1057-1066.

_____, 1970, "The Effective Reflection Coefficients in Forward Scatter from a Dielectric Slightly Rough Surface," Proc. IEEE 58:1279.

_____, et al., 1972, "Comments on 'The Relationship between the Kirchhoff Approach and Small Perturbation Analysis in Rough Surface Scattering Theory,'" IEEE Trans. AP-21:536-539.

Valyus, N. A., 1966, *Stereoscopy* (Focal Press).

Weyl, H., 1919, "Ausbreitung elektromagnetischer wellen über einen ebenen leiter," Ann. Phys. 60:481-500.

Wolf, E., 1970, "Determination of the Amplitude and the Phase of Scattered Fields by Holography," J. Opt. Soc. Am. 60:18-20.